Journal of Thermal Stresses
Publication details, including instructions for authors and subscription information:
http://www.tandfonline.com/loi/uths20

Thermal Stability of FGM Sandwich Plates Under Various Through-the-Thickness Temperature Distributions

F. A. Fazzolari [a] & E. Carrera [b]

[a] School of Engineering and Mathematical Sciences , City University London , London , United Kingdom

[b] Department of Mechanical and Aerospace Engineering , Politecnico di Torino , Torino , Italy

Published online: 10 Sep 2014.

Journal of Thermal Stresses, 37: 1449–1481, 2014

ISSN: 0149-5739 print/1521-074X online
DOI: 10.1080/01495739.2014.937251

Taylor & Francis
Taylor & Francis Group

THERMAL STABILITY OF FGM SANDWICH PLATES UNDER VARIOUS THROUGH-THE-THICKNESS TEMPERATURE DISTRIBUTIONS

F. A. Fazzolari[1] and E. Carrera[2]

[1]*School of Engineering and Mathematical Sciences, City University London, London, United Kingdom*

[2]*Department of Mechanical and Aerospace Engineering, Politecnico di Torino, Torino, Italy*

A thermal stability analysis of functionally graded material (FGM) isotropic and sandwich plates is carried out by virtue of a refined quasi-3D Equivalent Single Layer (ESL) and Zig-Zag (ZZ) plate models developed within the framework of the Carrera Unified Formulation (CUF) and implemented within the Hierarchical Trigonometric Ritz Formulation (HTRF). The Principle of Virtual Displacements (PVD) is used both to derive the thermal stability differential equations with natural boundary conditions and to develop the HTRF. Uniform, linear, and non-linear temperature rises through-the-thickness direction are taken into account. The non-linear temperature distribution is given in different forms: 1) functionally graded; 2) solution of the one-dimensional Fourier heat conduction equation; and 3) sinusoidal. Several FGM sandwich plate configurations are investigated. Parametric studies are carried out in order to evaluate the effects of significant parameters, such as volume fraction index, length-to-thickness ratio, boundary conditions, aspect ratio, sandwich plate type, and temperature distribution through-the-thickness direction, on the critical buckling temperatures.

Keywords: Advanced hierarchical plate theories; FGM isotropic and sandwich plates; Non-linear temperature distribution; Thermal buckling; Trigonometric Ritz formulation

INTRODUCTION

Aerospace structures often experience severe loading conditions. During their operations, life aerospace structures are subjected to both aerodynamic loads, which depend on aerodynamic pressure distributions and viscous forces, and aero-thermal effects, which take into account surface heating-rate and inner temperature distributions. The rise of temperature due to aerodynamic heating strongly decreases the structural load-bearing capacity affecting the buckling phenomena. It becomes mandatory for design engineers to carry out their thermal stability analysis

Received 31 January 2014; accepted 6 April 2014.

Address correspondence to Fiorenzo Fazzolari, Aeronautics, Astronautics and Computational Engineering Academic Unit, University of Southampton, Boldrewood Campus, Southampton, SO16 7QF, UK. E-mail: F.Fazzolari@soton.ac.uk

Color versions of one or more of the figures in the article can be found online at www.tandfonline.com/uths.

to prevent failures. The thermal buckling phenomenon has been thoroughly investigated during the past decades.

A comprehensive literature review concerning thermal buckling has been given by Thornton [1] and Tauchert [2], where thermal effects upon flexure, buckling and vibration of plates and shells were presented. Gray and Mei [3] investigated the thermal post-buckling behavior and free vibration of thermally buckled composite plates using the Finite Element Method (FEM).

Probably the first analyses of thermal buckling of shear deformable laminated plates are included in the work of Tauchert [4]. He used a First-order Shear Deformation Theory (FSDT) to analyze simply supported plates of antisymmetric angle-ply construction subjected to a uniform temperature rise. Yang and Sheih [5] employed the Galerkin method to investigate thermal buckling of initially stressed antisymmetric cross-ply plates. Chen et al. [6] considered both uniform and non-uniform temperature distributions using the FEM. Noor and Jeanne [7] used predictor-corrector procedures for thermal buckling analysis. Prabhu and Dhanaraj [8] considered symmetrically laminated plates with different boundary conditions in the thermal buckling analysis using FEM. A three-dimensional solution for composite and sandwich plates was provided by Noor et al. [9] and Noor and Burton [10]. Kant and Babu [11] dealt with the same problem by employing shear deformable finite element models. Other contributions that are referred to pure mechanical or pure thermal loadings can be found in [12–18]. Recently, Fazzolari and Carrera [19, 20] provided advanced Ritz, Galerkin and Generalized Galerkin formulations based on the use of quasi-3D hierarchical plate models to carry out thermomechanical buckling analysis of laminated composite and sandwich plates.

To deal with ultrahigh temperature applications a relatevely new class of materials referred to as Functionally Graded Materials (FGMs) was introduced. More specifically, FGMs represent a class of heterogeneous composite materials made up of a mixture of ceramics and metals that are characterized by the smooth and continuous variation in properties from the bottom to the top of the considered structural element. The material properties of FGMs are controlled by the variation of the volume fraction of the constituent materials. As ultrahigh temperature-resistant materials, they are suitable for aerospace applications, such as aircraft, space vehicles, barrier coating and propulsion systems. Thus, with their potential applications, FGMs are steadfastly making headway in aerospace design. Moreover, they have many advantages over other types of advanced materials like fiber-reinforced composites. Indeed, problems such as delamination, fiber failure, adverse hygroscopic effects due to moisture content, and more are effectively eliminated or are non-existent.

Many works have been devoted to investigate the static and dynamic thermal response of FGM structures. Zenkour and Sobhy [21] studied the thermal buckling of various types of FGM sandwich plates. Zhao et al. [22] carried out a mechanical and thermal buckling analysis of functionally graded ceramic-metal plates using the FSDT in conjunction with the element-free kp-Ritz. Thermal buckling of a simply supported moderately thick rectangular FGM plate was investigate by Lanhe [23]. Shen [24] dealt with the thermal postbuckling behavior of shear deformable FGM plates with temperature-dependent properties. Uymaz and Aydogdu [25] provided a three-dimensional shear buckling solution for FG plates with various boundary conditions. A three-dimensional thermal buckling analysis of functionally graded

arbitrary straight-sided quadrilateral plates using differential quadrature method has been given by Malekzadeh [26].

The buckling of thick functionally graded plates under mechanical and thermal loads was studied by Shariat and Eslami [27]. Both uniform and non-linear temperature rises through-the-thickness were considered, and the equilibrium and stability equations were derived using the Third-order Shear Deformation plate Theory (TSDT). The same authors [28] investigated the thermal buckling analysis of rectangular functionally graded plates (FGPs) with geometrical imperfections using the Classical Lamination plate Theory (CLT). Matsunaga [29] used a two-dimensional global Higher-order Shear Deformation Theory (HSDT) for the thermal buckling analysis of FGM plates, and the solution was given by using the method of power series expansion of displacement components.

In the present article the Hierarchical Trigonometric Ritz Formulation (HTRF), extensively employed in the analysis of laminated composite plates and shells [19, 20, 30–34], has been extended to the thermal stability of FGM sandwich plates. Advanced Equivalent Single Layer (ESL) and Zig-Zag (ZZ) plate models with hierarchical capabilities were employed and assessed by comparison with other results available in the literature. The accuracy of the proposed formulation has been thoroughly examined. Uniform, linear, and non-linear temperature rises through-the-thickness direction have been taken into account. Several FGM sandwich plate configurations have been investigated. Results are presented in terms of critical buckling temperatures. The effects of significant parameters, such as volume fraction index, length-to-thickness ratio, aspect ratio, boundary conditions, temperature distribution and FGM sandwich plate-type are discussed.

GEOMETRIC AND CONSTITUTIVE RELATIONS IN THERMOMECHANICAL PROBLEMS

The geometrical characteristics of the FGM isotropic and sandwich plates are shown in Figure 1. During the development of the proposed formulation some symbols have been introduced. In particular, the integer k, used as superscript or subscript, denotes the layer number that starts from the bottom of the plate. The layer geometry is denoted by the same symbols as those used for the whole FGM sandwich plate and vice-versa. The plate middle surface Ω_k coordinates are indicated by x and y; Γ_k is the layer boundary on Ω_k; z and z_k are the plate and layer thickness coordinates; h and h_k denote the plate and layer thicknesses, respectively; $\zeta_k = 2z_k/h_k$ is the dimensionless local layer-coordinate; A_k denotes the k-layer thickness domain $\left(A_k \in \left[z_k, z_{k+1}\right]\right)$. Symbols without the k subscript/superscripts refer to the whole plate. The notation for the displacement vector is

$$\mathbf{u} = \begin{bmatrix} u_x & u_y & u_z \end{bmatrix}^T \tag{1}$$

Superscript T represents the transposition operator. The stresses, $\boldsymbol{\sigma}$, and the strains, $\boldsymbol{\varepsilon}$, are expressed as follows:

$$\begin{aligned} \boldsymbol{\sigma}_{pH}^k &= \begin{bmatrix} \sigma_{xx}^k & \sigma_{yy}^k & \tau_{xy}^k \end{bmatrix}^T, \quad \boldsymbol{\varepsilon}_{pG}^k = \begin{bmatrix} \varepsilon_{xx}^k & \varepsilon_{yy}^k & \gamma_{xy}^k \end{bmatrix}^T \\ \boldsymbol{\sigma}_{nH}^k &= \begin{bmatrix} \tau_{xz}^k & \tau_{yz}^k & \sigma_{zz}^k \end{bmatrix}^T, \quad \boldsymbol{\varepsilon}_{nG}^k = \begin{bmatrix} \gamma_{xz}^k & \gamma_{yz}^k & \varepsilon_{zz}^k \end{bmatrix}^T \end{aligned} \tag{2}$$

The subscripts n and p denote transverse (out-of-plane) and in-plane components, respectively, and the subscripts H and G state that Hooke's law and geometric relations are used. The strain-displacement relations are

$$\begin{cases} \boldsymbol{\varepsilon}_{pG}^{k} = \mathbf{D}_{p}\mathbf{u}^{k} \\ \boldsymbol{\varepsilon}_{p_{nl}}^{k} = \mathbf{D}_{p_{nl}}\mathbf{u}^{k} \\ \boldsymbol{\varepsilon}_{nG}^{k} = \mathbf{D}_{n}\mathbf{u}^{k} = (\mathbf{D}_{np} + \mathbf{D}_{nz})\,\mathbf{u}^{k} \end{cases} \tag{3}$$

where $\mathbf{D}_p$, $\mathbf{D}_n$, $\mathbf{D}_{np}$ and $\mathbf{D}_{nz}$ are differential matrix operators defined as follows:

$$\begin{aligned} \mathbf{D}_p &= \begin{bmatrix} \frac{\partial}{\partial x} & 0 & 0 \\ 0 & \frac{\partial}{\partial y} & 0 \\ \frac{\partial}{\partial y} & \frac{\partial}{\partial x} & 0 \end{bmatrix}, \quad \mathbf{D}_n = \begin{bmatrix} \frac{\partial}{\partial z} & 0 & \frac{\partial}{\partial x} \\ 0 & \frac{\partial}{\partial z} & \frac{\partial}{\partial y} \\ 0 & 0 & \frac{\partial}{\partial z} \end{bmatrix} \\ \mathbf{D}_{np} &= \begin{bmatrix} 0 & 0 & \frac{\partial}{\partial x} \\ 0 & 0 & \frac{\partial}{\partial y} \\ 0 & 0 & 0 \end{bmatrix}, \quad \mathbf{D}_{nz} = \begin{bmatrix} \frac{\partial}{\partial z} & 0 & 0 \\ 0 & \frac{\partial}{\partial z} & 0 \\ 0 & 0 & \frac{\partial}{\partial z} \end{bmatrix} \end{aligned} \tag{4}$$

The 3D costitutive equations according to Hooke's law are given as

$$\boldsymbol{\sigma}^{k} = \mathbf{C}^{k}\boldsymbol{\varepsilon}^{k} \tag{5}$$

By using Eq. (2), the previous equation becomes

$$\begin{aligned} \boldsymbol{\sigma}_{pH}^{k} &= \widetilde{\mathbf{C}}_{pp}^{k}(z)\,\boldsymbol{\varepsilon}_{pG}^{k} + \widetilde{\mathbf{C}}_{pn}^{k}(z)\,\boldsymbol{\varepsilon}_{nG}^{k} \\ \boldsymbol{\sigma}_{nH}^{k} &= \widetilde{\mathbf{C}}_{np}^{k}(z)\,\boldsymbol{\varepsilon}_{pG}^{k} + \widetilde{\mathbf{C}}_{nn}^{k}(z)\,\boldsymbol{\varepsilon}_{nG}^{k} \end{aligned} \tag{6}$$

where matrices $\widetilde{\mathbf{C}}_{pp}^{k}(z)$, $\widetilde{\mathbf{C}}_{nn}^{k}(z)$, $\widetilde{\mathbf{C}}_{pn}^{k}(z)$ and $\widetilde{\mathbf{C}}_{np}^{k}(z)$ are

$$\begin{aligned} \widetilde{\mathbf{C}}_{pp}^{k}(z) &= \begin{bmatrix} \widetilde{C}_{11}(z) & \widetilde{C}_{12}(z) & 0 \\ \widetilde{C}_{12}(z) & \widetilde{C}_{22}(z) & 0 \\ 0 & 0 & \widetilde{C}_{66}(z) \end{bmatrix}^{k}, \quad \widetilde{\mathbf{C}}_{nn}^{k}(z) = \begin{bmatrix} \widetilde{C}_{55}(z) & 0 & 0 \\ 0 & \widetilde{C}_{44}(z) & 0 \\ 0 & 0 & \widetilde{C}_{33}(z) \end{bmatrix}^{k}, \\ \widetilde{\mathbf{C}}_{pn}^{k}(z) &= \begin{bmatrix} 0 & 0 & \widetilde{C}_{13}(z) \\ 0 & 0 & \widetilde{C}_{23}(z) \\ 0 & 0 & 0 \end{bmatrix}^{k}, \quad \widetilde{\mathbf{C}}_{np}^{k}(z) = \begin{bmatrix} 0 & 0 & 0 \\ 0 & 0 & 0 \\ \widetilde{C}_{13}(z) & \widetilde{C}_{23}(z) & 0 \end{bmatrix}^{k} \end{aligned} \tag{7}$$

In Eq. (7) the computation of the elastic coefficients $\widetilde{C}_{ij}$, is independent of the FGM structures considered, and it follows three steps:

1. Computation of volume fraction of ceramic and metal phases;
2. Computation of elastic properties, Young's modulus E^{k} and Poisson's coefficient ν^{k}; and,
3. Computation of elastic coefficients $\widetilde{C}_{ij}$.

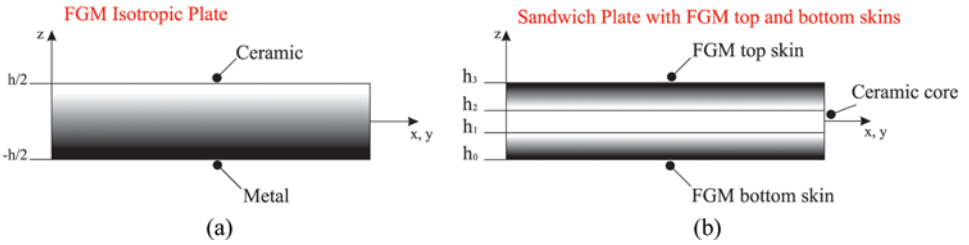

Figure 1 FGM isotropic and sandwich plates.

Only the computation of the volume fraction depends on the analyzed FGM structure. In the present investigation the following cases are examined:

1. FGM isotropic plates, the bottom skin is metal and the top skin is ceramic (see Figure 1a), the volume fraction of the ceramic phase is defined according to the following power law:

$$V_c^k(z) = \left(\frac{z}{h} + \frac{1}{2}\right)^p \quad z \in [-h/2,\ h/2] \tag{8}$$

   and it trends against the dimensionless thickness coordinate z/h is shown in Figure 2.
2. FGM sandwich plates, the core is fully ceramic and the top and bottom skins are FGM across the thickness direction (see Figure 1b). The volume fraction of the

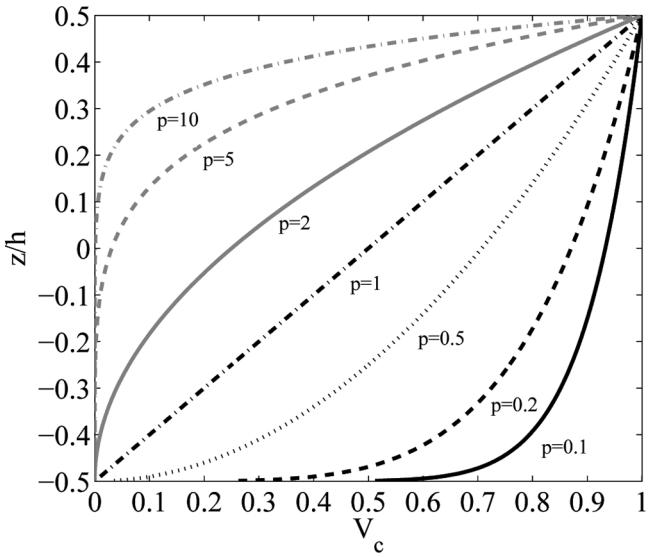

Figure 2 Volume fraction (V_c) distribution through-the-thickness plate direction for different values of the volume fraction index (p).

ceramic phase is defined according to the following power-law:

$$\begin{cases} V_c^k(z) = \left(\dfrac{z-h_0}{h_1-h_0}\right)^p & z \in [h_0,\ h_1] \\ V_c^k(z) = 1 & z \in [h_1,\ h_2] \\ V_c^k(z) = \left(\dfrac{z-h_3}{h_3-h_2}\right)^p & z \in [h_2,\ h_3] \end{cases} \tag{9}$$

and some trends, of several FGM sandwich plates, against the dimensionless thickness coordinate z/h, are shown in Figure 3.

In Eqs. (8) and (9), p indicates the volume fraction index indicating the material variation through-the-thickness direction. The volume fraction of the metal phase is given as $V_m^k(z) = 1 - V_c^k(z)$. Poisson's coefficient ν^k is constant through thickness direction; Young's modulus $E^k(z)$ and thermal expansion coefficient $\alpha^k(z)$ are

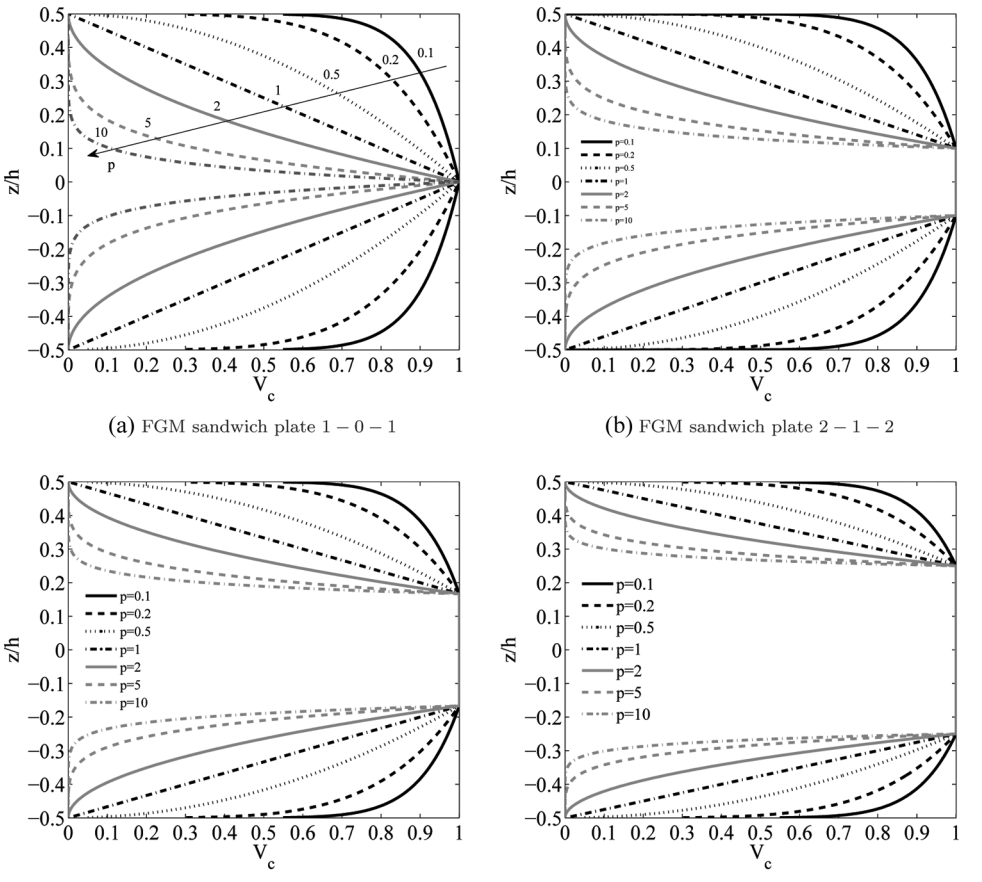

(a) FGM sandwich plate $1-0-1$ (b) FGM sandwich plate $2-1-2$

(c) FGM sandwich plate $1-1-1$ (d) FGM sandwich plate $1-2-1$

Figure 3 Volume fraction (V_c) distribution through-the-thickness plate direction for different values of the volume fraction index (p) and several FGM sandwich plate configurations.

computed by the following law-of-mixtures:

$$\begin{cases} E^k(z) = (E_c - E_m)\ V_c^k(z) + E_m \\ \alpha^k(z) = (\alpha_c - \alpha_m)\ V_c^k(z) + \alpha_m \\ v^k(z) = v_0 \end{cases} \tag{10}$$

Finally the elastic coefficients $\widetilde{C}_{ij}$ are given as

$$\begin{cases} \widetilde{C}_{11}^k(z) = \widetilde{C}_{22}^k(z) = \widetilde{C}_{33}^k(z) = \dfrac{E^k(z)\left[1 - \left(v^k(z)\right)^2\right]}{1 - 3\left(v^k(z)\right)^2 - 2\left(v^k(z)\right)^3} \\ \widetilde{C}_{12}^k(z) = \widetilde{C}_{12}^k(z) = \widetilde{C}_{23}^k(z) = \dfrac{E^k(z)\left[v^k(z) - \left(v^k(z)\right)^2\right]}{1 - 3\left(v^k(z)\right)^2 - 2\left(v^k(z)\right)^3} \\ \widetilde{C}_{44}^k(z) = \widetilde{C}_{55}^k(z) = \widetilde{C}_{66}^k(z) = \dfrac{E^k(z)}{2\left(1 + v^k(z)\right)} \end{cases} \tag{11}$$

Thermomechanical coupling coefficients expressed in the laminate reference system are

$$\begin{aligned} \boldsymbol{\lambda}_p^k(z) &= \widetilde{\mathbf{C}}_{pp}^k(z)\,\tilde{\boldsymbol{\alpha}}_p^k(z) + \widetilde{\mathbf{C}}_{pn}^k(z)\,\tilde{\boldsymbol{\alpha}}_n^k(z) \\ \boldsymbol{\lambda}_n^k(z) &= \widetilde{\mathbf{C}}_{np}^k(z)\,\tilde{\boldsymbol{\alpha}}_p^k(z) + \widetilde{\mathbf{C}}_{nn}^k(z)\,\tilde{\boldsymbol{\alpha}}_n^k(z) \end{aligned} \tag{12}$$

where

$$\tilde{\boldsymbol{\alpha}}_p^k = \begin{bmatrix} \alpha(z) \\ \alpha(z) \\ 0 \end{bmatrix}^k, \quad \tilde{\boldsymbol{\alpha}}_n^k = \begin{bmatrix} 0 \\ 0 \\ \alpha(z) \end{bmatrix}^k \tag{13}$$

are the thermal expansion coefficients split into in-plane and out-of-plane components. In the explicit vectorial form, the thermomechanical coupling coefficients are

$$\boldsymbol{\lambda}_p^k = \begin{bmatrix} \lambda(z) \\ \lambda(z) \\ 0 \end{bmatrix}^k, \quad \boldsymbol{\lambda}_n^k = \begin{bmatrix} 0 \\ 0 \\ \lambda(z) \end{bmatrix}^k \tag{14}$$

The initial thermal stresses can be defined as

$$\sigma_{xx_0}^{\vartheta^k} = \lambda^k\,\Delta T; \quad \sigma_{yy_0}^{\vartheta^k} = \lambda^k\,\Delta T; \quad \sigma_{zz_0}^{\vartheta^k} = \lambda^k\,\Delta T \tag{15}$$

where ΔT is the temperature rise through-the-thickness direction and λ is the coefficient relating thermal stresses to temperature variation. After imposing the plane stress assumptions, the initial thermal stresses assume the following form:

$$\tilde{\sigma}_{xx_0}^{\vartheta^k} = \tilde{\lambda}^k\,\Delta T; \quad \tilde{\sigma}_{yy_0}^{\vartheta^k} = \tilde{\lambda}^k\,\Delta T \tag{16}$$

A comprehensive discussion on the initial thermal stresses with the explicit expression of the transformed thermomechanical coupling coefficients $\tilde{\lambda}^k$, can be found in [33].

UNIFORM, LINEAR, AND NON-LINEAR TEMPERATURE RISES THROUGH-THE-THICKNESS DIRECTION

To accurately describe the effects of the temperature rise through-the-thickness different temperature distributions (see Figure 4) are taken into account in the present analysis. In particular, uniform, linear and non-linear temperature distributions are accounted for in the proposed investigation. In the non-linear case, the temperature rise is given as: i) functionally graded, encompassing therefore uniform and linear distributions; ii) the solution of the one-dimensional Fourier equation of heat conduction; and, iii) sinusoidal. Each case is accurately described in the following subsections.

Uniform Temperature Rise

The plate initial temperature is assumed to be T_i. The temperature is uniformly raised to a final value T_f in which the plate buckles. The temperature change is given by

$$\Delta T = T_f - T_i \tag{17}$$

Linear Temperature Rise

The temperature of the top surface is T_t and it is considered to vary linearly from T_t to the bottom surface temperature T_b. Therefore, the temperature rise

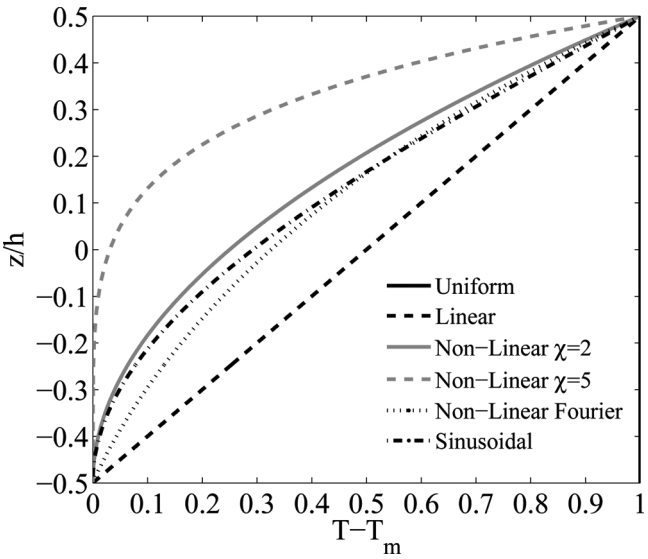

Figure 4 Temperature distributions through-the-thickness direction.

through-the-thickness is given by

$$T(z) = \Delta T\left(\frac{z}{h} + \frac{1}{2}\right) + T_b \tag{18}$$

where $\Delta T = T_t - T_b$.

Non-Linear Temperature Rise

In this case, the temperature distribution through-the-thickness has been given according to the following three approaches:

1. In the first case, the temperature of the top surface is T_t and it is considered to vary from T_t to T_b in which the plate buckles, according to the power law variation through-the-thickness, to the bottom surface temperature T_b in which the plate buckles. Therefore, the temperature rise through-the-thickness is given by

$$T(z) = \Delta T\left(\frac{z}{h} + \frac{1}{2}\right)^{\chi} + T_b \tag{19}$$

   where χ is the temperature index $0 < \chi < \infty$. The linear temperature rise is obtained as a particular case by setting $\chi = 1$.
2. In the second case, the one-dimensional Fourier equation of heat conduction,

$$\begin{cases} \dfrac{\mathrm{d}}{\mathrm{d}z}\left[K(z)\dfrac{\mathrm{d}T}{\mathrm{d}z}\right] = 0 & -h/2 < z < h/2 \\ T = T_c & z = h/2 \\ T = T_m & z = -h/2 \end{cases} \tag{20}$$

   is solved. $K(z)$ is the coefficient of thermal conduction, T_c and T_m denote the temperature changes at the ceramic side and the metal side, respectively. Similar to the coefficients of elastic moduli and thermal expansion, the coefficient of heat conduction is also assumed as a power form of coordinate variable z as

$$K(z) = (K_c - K_m)\ V_c^k + K_m \tag{21}$$

   Equation (20) can be solved by using a polynomial power series expansion given as

$$T(z) = T_m + \frac{(T_c - T_m)}{C}\left(\frac{z}{h} + \frac{1}{2}\right)\sum_{i=0}^{N_T}\left[(-1)^i\ \frac{\left(\frac{z}{h} + \frac{1}{2}\right)^{i\,p}\ (K_c - K_m)^i}{(i\,p+1)\ K_m}\right] \tag{22}$$

   where N_T is the number of series' terms, which for the case of non-uniform temperature rise is obtained from a convergence study. C is defined as follows:

$$C = \sum_{i=0}^{N_T}\left[(-1)^i\ \frac{(K_c - K_m)^i}{(i\,p+1)\ K_m}\right] \tag{23}$$

3. In the third case, the temperature distribution across the thickness direction follows a sinusoidal law as

$$T(z) = \Delta T \left\{ 1 - \cos \left[\frac{\pi}{2} \left(\frac{z}{h} + \frac{1}{2} \right) \right] \right\} + T_b \tag{24}$$

As can be seen from Figure 4 this distribution is encompassed in the envelope built between the Fourier's non-linear distribution and the parabolic functional graded distribution. It should be kept in mind that for thick FGM isotropic and sandwich plates, the critical temperature is higher than the melting point of the single constituents; hence, the thermal stability analysis can be restricted from thin-to-moderately thick FGM isotropic and sandwich plates.

HIERARCHICAL PLATE MODELS

In the analysis of metallic and composite plates and shells the 3D elastic problem is generally reduced to a two-dimensional one by exploiting the use of axiomatic assumptions coming from some pioneering insights due to eminent scientists and researchers. The simplest plate/shell theory is based on the Kirchhoff/Love's hypothesis, and it is usually referred to as Classical Lamination Theory (CLT) [35, 36]. Both transverse shear strains and transverse normal strains are discarded, in usual applications being negligible with respect to the in-plane ones,

$$\begin{cases} u_x(x, y, z) = u_{x0}(x, y) - z \dfrac{\partial u_{z0}(x, y)}{\partial x} \\ u_y(x, y, z) = u_{y0}(x, y) - z \dfrac{\partial u_{z0}(x, y)}{\partial y} \\ u_z(x, y, z) = u_{z0}(x, y) \end{cases} \tag{25}$$

The inclusion of transverse shear strains, in the theory mentioned here, leads to Reissner–Mindlin Theory, also known as First-order Shear Deformation Theory (FSDT) [37, 38],

$$\begin{cases} u_x(x, y, z) = u_{x0}(x, y) + z\, u_{x1}(x, y) \\ u_y(x, y, z) = u_{y0}(x, y) + z\, u_{y1}(x, y) \\ u_z(x, y, z) = u_{z0}(x, y) \end{cases} \tag{26}$$

However, these theories, due to their inconsistency in discarding the transverse normal stress in the material constitutive equations, are no longer valid when 3D local effects appear. To remove the inconsistency completely, higher-order expansion of the unknown with respect to the z coordinate are needed. According to the preceding considerations, CUF, well known in the statics and dynamics analysis of layered beams, plates and shells, overcomes the drawback by generating a large variety of 2D and quasi-3D hierarchical plate/shell models using a unified approach. Its accuracy has been proved in many applications ranging from multifield to aeroelastic problems, and it turned out to be a powerful tool to deal with metallic and composite laminated beams, plates and shells. The capability to expand each

displacement variable in the displacement field at any desired order independently from the others and with respect to the accuracy and the computational cost has been introduced. Such an artifice permits us to treat each variable independently from the others. This becomes extremely useful when multifield problems are investigated such as thermoelastic and piezoelectric applications [31, 39]. Thereby, following this approach the displacement field can be written as

$$\begin{cases} u_x(x,y,z) = F_{\tau_{u_x}}(z)\, u_{x\tau_{u_x}}(x,y), & \tau_{u_x} = 0, 1, \cdots, N_{u_x} \\ u_y(x,y,z) = F_{\tau_{u_y}}(z)\, u_{y\tau_{u_y}}(x,y), & \tau_{u_y} = 0, 1, \cdots, N_{u_y} \\ u_z(x,y,z) = F_{\tau_{u_z}}(z)\, u_{z\tau_{u_z}}(x,y), & \tau_{u_z} = 0, 1, \cdots, N_{u_z} \end{cases} \tag{27}$$

and in compact form:

$$\mathbf{u} = \mathbf{F}_\tau \mathbf{u}_\tau, \quad \tau = \tau_{u_x}, \tau_{u_y}, \tau_{u_z} \tag{28}$$

where

$$\mathbf{F}_\tau = \begin{bmatrix} F_{\tau_{u_x}} & 0 & 0 \\ 0 & F_{\tau_{u_y}} & 0 \\ 0 & 0 & F_{\tau_{u_z}} \end{bmatrix}, \quad \mathbf{u}_\tau = \begin{Bmatrix} u_{x\tau_{u_x}} \\ u_{y\tau_{u_y}} \\ u_{z\tau_{u_z}} \end{Bmatrix} \tag{29}$$

$u_{x\tau_{u_x}}$, $u_{y\tau_{u_y}}$, $u_{z\tau_{u_z}}$ are the displacement vector components and N_{u_x}, N_{u_y} and N_{u_z} are the orders of expansion. According to Einstein's notation, the repeated subscripts τ_{u_x}, τ_{u_y}, τ_{u_z} indicate summation. An example of a possible ESL displacement field according to the unified formulation in Eq. (27) is given below, the expansion indexes are $N_{u_x} = 6$, $N_{u_y} = 2$, $N_{u_z} = 4$:

$$\begin{cases} u_x = u_{x_0} + z\, u_{x1} + z^2\, u_{x2} + z^3\, u_{x3} + z^4\, u_{x4} + z^5\, u_{x5} + z^6\, u_{x6} \\ u_y = u_{y_0} + z\, u_{y1} + z^2\, u_{y2} \\ u_z = u_{z_0} + z\, u_{z1} + z^2\, u_{z2} + z^3\, u_{z3} + z^4\, u_{z4} \end{cases} \tag{30}$$

An exhaustive and comprehensive coverage, along with some clarifying illustrations about the ESL, ZZ as well as LW (Layer-Wise) assembly procedures from layer to multilayer are available in [32].

Classical models violate interlaminar equilibrium of the transverse stresses. Further they do not describe the ZZ form of the displacement field in the plate thickness direction. Such a limitation could somehow be overcome by referring to Murakami's idea. Murakami [40] proposed adding a *ZZ* function to Eq. (27),

$$\begin{cases} u_x = u_{x_0} + z^{r_{u_x}}\, u_{xr_{u_x}} + u_{Z_{u_x}}\, (-1)^k\, \zeta_k, & r_{u_x} = 1, 2, \ldots, N_{u_x} - 1 \\ u_y = u_{y_0} + z^{r_{u_y}}\, u_{yr_{u_y}} + u_{Z_{u_y}}\, (-1)^k\, \zeta_k, & r_{u_y} = 1, 2, \ldots, N_{u_y} - 1 \\ u_z = u_{z_0} + z^{r_{u_z}}\, u_{zr_{u_z}} + u_{Z_{u_z}}\, (-1)^k\, \zeta_k, & r_{u_z} = 1, 2, \ldots, N_{u_z} - 1 \end{cases} \tag{31}$$

Subscript Z refers to the introduced *ZZ* term. Murakami's ZZ function (MZZF) is defined as $M(z) = (-1)^k\, \zeta_k$. Such a function permits one to reproduce the

discontinuity of the first derivative of the displacement variables in the z-direction, which physically comes from the intrinsic transverse anisotropy of multilayer structures.

THEORETICAL FORMULATION

In the following derivation the Principle of Virtual Displacements (PVD) is employed both to derive the thermal stability differential equations with related natural boundary conditions and to develop the Hierarchical Trigonometric Ritz Formulation (HTRF). The PVD variational statement [19, 41], in the case of thermal stability analysis at the multilayer level can be written as

$$\sum_{k=1}^{N_l} \int_{\Omega^k} \int_{A^k} \left(\delta \boldsymbol{\varepsilon}_{pG}^{k\,T} \boldsymbol{\sigma}_{pC}^{k} + \delta \boldsymbol{\varepsilon}_{nG}^{k\,T} \boldsymbol{\sigma}_{nC}^{k} \right) \mathrm{d}\Omega^k \, \mathrm{d}z = \sum_{k=1}^{N_l} \delta L_{ext}^{k} \tag{32}$$

where L_{ext}^{k} is the work carried out by the external forces at k-layer level. The HTRF herein proposed for thermal buckling analysis of FGM isotropic and sandwich plates is based on the so-called Ritz fundamental primary and secondary nuclei, which can be developed in a systematic manner following some steps proposed by the authors in [33]. In particular, in the Ritz method the displacement amplitude vector components $u_{x_{\tau_{u_x}}}$, $u_{y_{\tau_{u_y}}}$, and $u_{z_{\tau_{u_z}}}$ are expressed in series expansion as follows:

$$u_{x_{\tau_{u_x}}} = \sum_{i}^{\mathcal{N}} U_{x\tau_{u_x} i}^{k} \psi_{x_i}, \quad u_{y_{\tau_{u_y}}} = \sum_{i}^{\mathcal{N}} U_{y\tau_{u_y} i}^{k} \psi_{y_i}, \quad u_{z_{\tau_{u_z}}} = \sum_{i}^{\mathcal{N}} U_{z\tau_{u_z} i}^{k} \psi_{z_i} \tag{33}$$

where $\mathcal{N}$ indicates the order of expansion in the approximation. $U_{x\tau_{u_x} i}$, $U_{y\tau_{u_y} i}$, $U_{z\tau_{u_z} i}$ are the unknown coefficients, ψ_{x_i}, ψ_{y_i}, ψ_{z_i} are the Ritz functions appropriately selected making reference to the features of the analyzed problem. Convergence to the exact solution is guaranteed if the basis functions are admissible functions in the used variational principle [19, 42, 43]. The displacement field is then given as

$$u_x = \sum_{i}^{\mathcal{N}} F_{\tau_{u_x}} U_{x\tau_{u_x} i} \psi_{x_i}, \quad u_y = \sum_{i}^{\mathcal{N}} F_{\tau_{u_y}} U_{y\tau_{u_y} i} \psi_{y_i}, \quad u_z = \sum_{i}^{\mathcal{N}} F_{\tau_{u_z}} U_{z\tau_{u_z} i} \psi_{z_i} \tag{34}$$

or in compact form:

$$\mathbf{u}^k = \mathbf{F}_\tau \, \mathbf{U}_{\tau i} \, \boldsymbol{\Psi}_i \tag{35}$$

where

$$\mathbf{U}_{\tau i}^{k} = \begin{bmatrix} U_{x\tau_{u_x} i}^{k} \\ U_{y\tau_{u_y} i}^{k} \\ U_{z\tau_{u_z} i}^{k} \end{bmatrix}, \quad \boldsymbol{\Psi}_i = \begin{bmatrix} \psi_{x_i} & 0 & 0 \\ 0 & \psi_{y_i} & 0 \\ 0 & 0 & \psi_{z_i} \end{bmatrix}, \quad \mathbf{F}_\tau = \begin{bmatrix} F_{\tau_{u_x}} & 0 & 0 \\ 0 & F_{\tau_{u_y}} & 0 \\ 0 & 0 & F_{\tau_{u_z}} \end{bmatrix} \tag{36}$$

By writing stresses and strains in terms of displacement components given in Eq. (3) and substituting them in Eq. (32) the explicit expressions of the internal virtual

work and the virtual work done by the external forces in terms of Ritz functions and unknown coefficients are obtained:

$$\begin{aligned}\delta L^k_{int} = \int_{\Omega^k}\int_{A^k} \delta \mathbf{U}^T_{\tau i} \Big(& \left[\mathbf{D}_p\left(\mathbf{F}_\tau \boldsymbol{\Psi}_i\right)\right]^T \left[\tilde{\boldsymbol{C}}^k_{pp}\mathbf{D}_p\left(\mathbf{F}_s \boldsymbol{\Psi}_j\right) + \tilde{\boldsymbol{C}}^k_{pn}\mathbf{D}_{np}\left(\mathbf{F}_s \boldsymbol{\Psi}_j\right) + \tilde{\boldsymbol{C}}^k_{pn}\mathbf{D}_{nz}\left(\mathbf{F}_s \boldsymbol{\Psi}_j\right)\right] \\ & + \left[\mathbf{D}_{np}\left(\mathbf{F}_\tau \boldsymbol{\Psi}_i\right)\right]^T \left[\tilde{\boldsymbol{C}}^k_{np}\mathbf{D}_p\left(\mathbf{F}_s \boldsymbol{\Psi}_j\right) + \tilde{\boldsymbol{C}}^k_{nn}\mathbf{D}_{np}\left(\mathbf{F}_s \boldsymbol{\Psi}_j\right) + \tilde{\boldsymbol{C}}^k_{nn}\mathbf{D}_{nz}\left(\mathbf{F}_s \boldsymbol{\Psi}_j\right)\right] \\ & + \left[\mathbf{D}_{nz}\left(\mathbf{F}_\tau \boldsymbol{\Psi}_i\right)\right]^T \left[\tilde{\boldsymbol{C}}^k_{np}\mathbf{D}_p\left(\mathbf{F}_s \boldsymbol{\Psi}_j\right) + \tilde{\boldsymbol{C}}^k_{nn}\mathbf{D}_{np}\left(\mathbf{F}_s \boldsymbol{\Psi}_j\right) + \tilde{\boldsymbol{C}}^k_{nn}\mathbf{D}_{nz}\left(\mathbf{F}_s \boldsymbol{\Psi}_j\right)\right] \Big) \\ & \times \mathbf{U}^k_{sj}\, \mathrm{d}\Omega^k\, \mathrm{d}z \\ \delta L^k_{ext} = \int_{\Omega^k}\int_{A^k} \delta \mathbf{U}^T_{\tau i} & \left[\left(\mathbf{F}_\tau \mathbf{F}_s\right)^T \boldsymbol{\Phi}\right] \mathbf{U}_{sj}\, \mathrm{d}\Omega^k\, \mathrm{d}z \end{aligned} \tag{37}$$

The matrix $\boldsymbol{\Phi} = \mathrm{diag}\left(\Phi_{11}, \Phi_{22}, \Phi_{33}\right)$, where

$$\begin{cases} \Phi_{11} = \tilde{\sigma}^{\vartheta}_{xx_0}\, \psi_{x_i,x}\, \psi_{x_j,x} + \tilde{\sigma}^{\vartheta}_{yy_0}\, \psi_{x_i,y}\, \psi_{x_j,y} \\ \Phi_{22} = \tilde{\sigma}^{\vartheta}_{xx_0}\, \psi_{y_i,x}\, \psi_{y_j,x} + \tilde{\sigma}^{\vartheta}_{yy_0}\, \psi_{y_i,y}\, \psi_{y_j,y} \\ \Phi_{33} = \tilde{\sigma}^{\vartheta}_{xx_0}\, \psi_{z_i,x}\, \psi_{z_j,x} + \tilde{\sigma}^{\vartheta}_{yy_0}\, \psi_{z_i,y}\, \psi_{z_j,y} \end{cases} \tag{38}$$

The quadratic forms in Eqs. (37) lead to the Ritz fundamental primary stiffness and initial stress nuclei:

$$\begin{aligned}\mathbf{K}^{k\tau s i j} = \int_{\Omega^k}\int_{A^k} \Big(& \left[\mathbf{D}_p\left(\mathbf{F}_\tau \boldsymbol{\Psi}_i\right)\right]^T \left[\tilde{\boldsymbol{C}}^k_{pp}\mathbf{D}_p\left(\mathbf{F}_s \boldsymbol{\Psi}_j\right) + \tilde{\boldsymbol{C}}^k_{pn}\mathbf{D}_{np}\left(\mathbf{F}_s \boldsymbol{\Psi}_j\right) + \tilde{\boldsymbol{C}}^k_{pn}\mathbf{D}_{nz}\left(\mathbf{F}_s \boldsymbol{\Psi}_j\right)\right] \\ & + \left[\mathbf{D}_{np}\left(\mathbf{F}_\tau \boldsymbol{\Psi}_i\right)\right]^T \left[\tilde{\boldsymbol{C}}^k_{np}\mathbf{D}_p\left(\mathbf{F}_s \boldsymbol{\Psi}_j\right) + \tilde{\boldsymbol{C}}^k_{nn}\mathbf{D}_{np}\left(\mathbf{F}_s \boldsymbol{\Psi}_j\right) + \tilde{\boldsymbol{C}}^k_{nn}\mathbf{D}_{nz}\left(\mathbf{F}_s \boldsymbol{\Psi}_j\right)\right] \\ & + \left[\mathbf{D}_{nz}\left(\mathbf{F}_\tau \boldsymbol{\Psi}_i\right)\right]^T \left[\tilde{\boldsymbol{C}}^k_{np}\mathbf{D}_p\left(\mathbf{F}_s \boldsymbol{\Psi}_j\right) + \tilde{\boldsymbol{C}}^k_{nn}\mathbf{D}_{np}\left(\mathbf{F}_s \boldsymbol{\Psi}_j\right) + \tilde{\boldsymbol{C}}^k_{nn}\mathbf{D}_{nz}\left(\mathbf{F}_s \boldsymbol{\Psi}_j\right)\right] \Big)\, \mathrm{d}\Omega^k\, \mathrm{d}z \\ \mathbf{K}^{k\tau s i j}_{\sigma} = \int_{\Omega^k}\int_{A^k} & \left[\left(\mathbf{F}_\tau \mathbf{F}_s\right)^T \boldsymbol{\Phi}\right] \mathrm{d}\Omega^k\, \mathrm{d}z \end{aligned} \tag{39}$$

At this stage, it is useful to introduce the following thickness and in-plane integrals in order to write in a concise manner the explicit form of the Ritz fundamental secondary nuclei:

$$\begin{aligned} J^{k\tau s} &= \int_{A^k} F_\tau F_s\, \mathrm{d}z, \quad J^{k\tau_z s} = \int_{A^k} \frac{\partial F_\tau}{\partial z} F_s\, \mathrm{d}z, \\ J^{k\tau s_z} &= \int_{A^k} F_\tau \frac{\partial F_s}{\partial z}\, \mathrm{d}z, \quad J^{k\tau_z s_z} = \int_{A^k} \frac{\partial F_\tau}{\partial z}\frac{\partial F_s}{\partial z}\, \mathrm{d}z \end{aligned} \tag{40}$$

where $\tau = \tau_{u_x}, \tau_{u_y}, \tau_{u_z}$, and $s = s_{u_x}, s_{u_y}, s_{u_z}$. Concerning the in-plane integrals it is convenient to rewrite the trial functions $\psi_{x_i}, \psi_{y_i}, \psi_{z_i}$ as

$$\begin{cases} \psi_{x_i}(x,y) = \sum_m \sum_n \phi^{u_x}_m(x)\, \phi^{u_x}_n(y) \\ \psi_{y_i}(x,y) = \sum_m \sum_n \phi^{u_y}_m(x)\, \phi^{u_y}_n(y) \\ \psi_{z_i}(x,y) = \sum_m \sum_n \phi^{u_z}_m(x)\, \phi^{u_z}_n(y) \end{cases} \tag{41}$$

by exploiting the use of Eq. (41) the general in-plane integrals can be written as

$$
\begin{aligned}
{}^{i}_{j}I^{\xi\zeta}_{mp} &= \int_0^a \frac{\mathrm{d}^{\xi}\phi^{i}_{m}(x)}{\mathrm{d}x^{\xi}} \frac{\mathrm{d}^{\zeta}\phi^{j}_{p}(x)}{\mathrm{d}x^{\zeta}}\mathrm{d}x \quad m = \cdots, M, \quad p = 1, \cdots, P \\
{}^{i}_{j}I^{\xi\zeta}_{nq} &= \int_0^b \frac{\mathrm{d}^{\xi}\phi^{i}_{n}(y)}{\mathrm{d}y^{\xi}} \frac{\mathrm{d}^{\zeta}\phi^{j}_{q}(y)}{\mathrm{d}y^{\zeta}}\mathrm{d}y \quad n = \cdots, N, \quad q = 1, \cdots, Q
\end{aligned}
\tag{42}
$$

where $i, j = u_x, u_y, u_z$ and ξ, ζ are differentiation orders. The trial functions in Eq. (41) are chosen to satisfy the simply supported and fully clamped boundary conditions. Therefore, considering Eqs. (40) and (42), the explicit forms of the Ritz secondary fundamental stiffness and mass nuclei are reported as follows (more details can be found in [20, 31, 33]):

$$
\begin{aligned}
K^{\tau_{u_x} s_{u_x}}_{u_x u_x} &= \widetilde{C}^{k}_{11}\, J^{k\tau_{u_x} s_{u_x}}\, {}^{u_x}_{u_x}I^{11}_{mp}\, {}^{u_x}_{u_x}I^{00}_{nq} + \widetilde{C}^{k}_{16}\, J^{k\tau_{u_x} s_{u_x}}\, {}^{u_x}_{u_x}I^{10}_{mp}\, {}^{u_x}_{u_x}I^{01}_{nq} + \widetilde{C}^{k}_{16}\, J^{k\tau_{u_x} s_{u_x}}\, {}^{u_x}_{u_x}I^{01}_{mp}\, {}^{u_x}_{u_x}I^{10}_{nq} \\
&\quad + \widetilde{C}^{k}_{66}\, J^{k\tau_{u_x} s_{u_x}}\, {}^{u_x}_{u_x}I^{00}_{mp}\, {}^{u_x}_{u_x}I^{11}_{nq} + \widetilde{C}^{k}_{55}\, J^{k\tau_{u_{x,z}} s_{u_{x,z}}}\, {}^{u_x}_{u_x}I^{00}_{mp}\, {}^{u_x}_{u_x}I^{00}_{nq} \\
K^{\tau_{u_x} s_{u_y}}_{u_x u_y} &= \widetilde{C}^{k}_{16}\, J^{k\tau_{u_x} s_{u_y}}\, {}^{u_x}_{u_y}I^{11}_{mp}\, {}^{u_x}_{u_y}I^{00}_{nq} + \widetilde{C}^{k}_{12}\, J^{k\tau_{u_x} s_{u_y}}\, {}^{u_x}_{u_y}I^{10}_{mp}\, {}^{u_x}_{u_y}I^{01}_{nq} + \widetilde{C}^{k}_{66}\, J^{k\tau_{u_x} s_{u_y}}\, {}^{u_x}_{u_y}I^{01}_{mp}\, {}^{u_x}_{u_y}I^{10}_{nq} \\
&\quad + \widetilde{C}^{k}_{26}\, J^{k\tau_{u_x} s_{u_y}}\, {}^{u_x}_{u_y}I^{00}_{mp}\, {}^{u_x}_{u_y}I^{11}_{nq} + \widetilde{C}^{k}_{45}\, J^{k\tau_{u_{x,z}} s_{u_{y,z}}}\, {}^{u_x}_{u_y}I^{00}_{mp}\, {}^{u_x}_{u_y}I^{00}_{nq} \\
K^{\tau_{u_x} s_{u_z}}_{u_x u_z} &= \widetilde{C}^{k}_{55}\, J^{k\tau_{u_{x,z}} s_{u_z}}\, {}^{u_x}_{u_z}I^{01}_{mp}\, {}^{u_x}_{u_z}I^{10}_{nq} + \widetilde{C}^{k}_{45}\, J^{k\tau_{u_{x,z}} s_{u_z}}\, {}^{u_x}_{u_z}I^{00}_{mp}\, {}^{u_x}_{u_z}I^{01}_{nq} + \widetilde{C}^{k}_{13}\, J^{k\tau_{u_x} s_{u_{z,z}}}\, {}^{u_x}_{u_z}I^{10}_{mp}\, {}^{u_x}_{u_z}I^{00}_{nq} \\
&\quad + \widetilde{C}^{k}_{36}\, J^{k\tau_{u_x} s_{u_{z,z}}}\, {}^{u_x}_{u_z}I^{00}_{mp}\, {}^{u_x}_{u_z}I^{10}_{nq} \\
K^{\tau_{u_y} s_{u_x}}_{u_y u_x} &= \widetilde{C}^{k}_{16}\, J^{k\tau_{u_y} s_{u_x}}\, {}^{u_y}_{u_x}I^{11}_{mp}\, {}^{u_y}_{u_x}I^{00}_{nq} + \widetilde{C}^{k}_{12}\, J^{k\tau_{u_y} s_{u_x}}\, {}^{u_y}_{u_x}I^{01}_{mp}\, {}^{u_y}_{u_x}I^{10}_{nq} + \widetilde{C}^{k}_{66}\, J^{k\tau_{u_y} s_{u_x}}\, {}^{u_y}_{u_x}I^{10}_{mp}\, {}^{u_y}_{u_x}I^{01}_{nq} \\
&\quad + \widetilde{C}^{k}_{26}\, J^{k\tau_{u_y} s_{u_x}}\, {}^{u_y}_{u_x}I^{00}_{mp}\, {}^{u_y}_{u_x}I^{11}_{nq} + \widetilde{C}^{k}_{45}\, J^{k\tau_{u_{y,z}} s_{u_{x,z}}}\, {}^{u_y}_{u_x}I^{00}_{mp}\, {}^{u_y}_{u_x}I^{00}_{nq} \\
K^{\tau_{u_y} s_{u_y}}_{u_y u_y} &= \widetilde{C}^{k}_{26}\, J^{k\tau_{u_y} s_{u_y}}\, {}^{u_y}_{u_y}I^{01}_{mp}\, {}^{u_y}_{u_y}I^{10}_{nq} + \widetilde{C}^{k}_{22}\, J^{k\tau_{u_y} s_{u_y}}\, {}^{u_y}_{u_y}I^{00}_{mp}\, {}^{u_y}_{u_y}I^{11}_{nq} + \widetilde{C}^{k}_{66}\, J^{k\tau_{u_y} s_{u_y}}\, {}^{u_y}_{u_y}I^{01}_{mp}\, {}^{u_y}_{u_y}I^{10}_{nq} \\
&\quad + \widetilde{C}^{k}_{26}\, J^{k\tau_{u_y} s_{u_y}}\, {}^{u_y}_{u_y}I^{00}_{mp}\, {}^{u_y}_{u_y}I^{11}_{nq} + \widetilde{C}^{k}_{44}\, J^{k\tau_{u_{y,z}} s_{u_{y,z}}}\, {}^{u_y}_{u_y}I^{00}_{mp}\, {}^{u_y}_{u_y}I^{00}_{nq}
\end{aligned}
\tag{43}
$$

$$
\begin{aligned}
K^{\tau_{u_y} s_{u_z}}_{u_y u_z} &= \widetilde{C}^{k}_{45}\, J^{k\tau_{u_{y,z}} s_{u_z}}\, {}^{u_y}_{u_z}I^{01}_{mp}\, {}^{u_y}_{u_z}I^{00}_{nq} + \widetilde{C}^{k}_{44}\, J^{k\tau_{u_{y,z}} s_{u_z}}\, {}^{u_y}_{u_z}I^{00}_{mp}\, {}^{u_y}_{u_z}I^{01}_{nq} + \widetilde{C}^{k}_{36}\, J^{k\tau_{u_y} s_{u_{z,z}}}\, {}^{u_y}_{u_z}I^{10}_{mp}\, {}^{u_y}_{u_z}I^{00}_{nq} \\
&\quad + \widetilde{C}^{k}_{23}\, J^{k\tau_{u_y} s_{u_{z,z}}}\, {}^{u_y}_{u_z}I^{00}_{mp}\, {}^{u_y}_{u_z}I^{10}_{nq} \\
K^{\tau_{u_z} s_{u_x}}_{u_z u_x} &= \widetilde{C}^{k}_{55}\, J^{k\tau_{u_z} s_{u_{x,z}}}\, {}^{u_z}_{u_x}I^{01}_{mp}\, {}^{u_z}_{u_x}I^{00}_{nq} + \widetilde{C}^{k}_{45}\, J^{k\tau_{u_z} s_{u_{x,z}}}\, {}^{u_z}_{u_x}I^{00}_{mp}\, {}^{u_z}_{u_x}I^{01}_{nq} + \widetilde{C}^{k}_{13}\, J^{k\tau_{u_{z,z}} s_{u_x}}\, {}^{u_z}_{u_x}I^{10}_{mp}\, {}^{u_z}_{u_x}I^{00}_{nq} \\
&\quad + \widetilde{C}^{k}_{36}\, J^{k\tau_{u_{z,z}} s_{u_x}}\, {}^{u_z}_{u_x}I^{00}_{mp}\, {}^{u_z}_{u_x}I^{10}_{nq} \\
K^{\tau_{u_z} s_{u_y}}_{u_z u_y} &= \widetilde{C}^{k}_{45}\, J^{k\tau_{u_z} s_{u_{y,z}}}\, {}^{u_z}_{u_y}I^{01}_{mp}\, {}^{u_z}_{u_y}I^{00}_{nq} + \widetilde{C}^{k}_{44}\, J^{k\tau_{u_z} s_{u_{y,z}}}\, {}^{u_z}_{u_y}I^{00}_{mp}\, {}^{u_z}_{u_y}I^{01}_{nq} + \widetilde{C}^{k}_{36}\, J^{k\tau_{u_{z,z}} s_{u_y}}\, {}^{u_z}_{u_y}I^{10}_{mp}\, {}^{u_z}_{u_y}I^{00}_{nq} \\
&\quad + \widetilde{C}^{k}_{23}\, J^{k\tau_{u_{z,z}} s_{u_y}}\, {}^{u_z}_{u_y}I^{00}_{mp}\, {}^{u_z}_{u_y}I^{10}_{nq} \\
K^{\tau_{u_z} s_{u_z}}_{u_z u_z} &= \widetilde{C}^{k}_{45}\, J^{k\tau_{u_z} s_{u_z}}\, {}^{u_z}_{u_z}I^{01}_{mp}\, {}^{u_z}_{u_z}I^{10}_{nq} + \widetilde{C}^{k}_{44}\, J^{k\tau_{u_z} s_{u_z}}\, {}^{u_z}_{u_z}I^{00}_{mp}\, {}^{u_z}_{u_z}I^{11}_{nq} + \widetilde{C}^{k}_{55}\, J^{k\tau_{u_z} s_{u_z}}\, {}^{u_z}_{u_z}I^{11}_{mp}\, {}^{u_z}_{u_z}I^{00}_{nq} \\
&\quad + \widetilde{C}^{k}_{45}\, J^{k\tau_{u_z} s_{u_z}}\, {}^{u_z}_{u_z}I^{10}_{mp}\, {}^{u_z}_{u_z}I^{01}_{nq} + \widetilde{C}^{k}_{33}\, J^{k\tau_{u_{z,z}} s_{u_{z,z}}}\, {}^{u_z}_{u_z}I^{00}_{mp}\, {}^{u_z}_{u_z}I^{00}_{nq}
\end{aligned}
$$

$$K^{\tau_{u_x} s_{u_x}}_{\sigma_{u_x u_x}} = \sigma^{\vartheta}_{xx_0} \; J^{k\tau_{u_x} s_{u_x}} \; {}^{u_x}_{u_x}I^{11}_{mp} \; {}^{u_x}_{u_x}I^{00}_{nq} + \sigma^{\vartheta}_{yy_0} \; J^{k\tau_{u_x} s_{u_x}} \; {}^{u_x}_{u_x}I^{00}_{mp} \; {}^{u_x}_{u_x}I^{11}_{nq}$$

$$K^{\tau_{u_y} s_{u_y}}_{\sigma_{u_y u_y}} = \sigma^{\vartheta}_{xx_0} \; J^{k\tau_{u_y} s_{u_y}} \; {}^{u_y}_{u_y}I^{11}_{mp} \; {}^{u_y}_{u_y}I^{00}_{nq} + \sigma^{\vartheta}_{yy_0} \; J^{k\tau_{u_y} s_{u_y}} \; {}^{u_y}_{u_y}I^{00}_{mp} \; {}^{u_y}_{u_y}I^{11}_{nq}$$

$$K^{\tau_{u_z} s_{u_z}}_{\sigma_{u_z u_z}} = \sigma^{\vartheta}_{xx_0} \; J^{k\tau_{u_z} s_{u_z}} \; {}^{u_z}_{u_z}I^{11}_{mp} \; {}^{u_z}_{u_z}I^{00}_{nq} + \sigma^{\vartheta}_{yy_0} \; J^{k\tau_{u_z} s_{u_z}} \; {}^{u_z}_{u_z}I^{00}_{mp} \; {}^{u_z}_{u_z}I^{11}_{nq}$$

For elastic systems subjected to conservative forces the PVD can be identified with the principle of minimum total potential energy. In particular, it is possible to write

$$\delta L^k_{int} = \delta U^k, \quad \delta L^k_{ext} = -\delta V^k \tag{44}$$

where δU is the virtual potential strain energy and δV is the virtual potential energy related to the external forces. Then Eq. (32) can be written as

$$\delta U^k + \delta V^k = 0 \tag{45}$$

being

$$\Pi^k = U^k + V^k \tag{46}$$

the total potential energy functional, then Eq. (32) corresponds to a minimization of the functional

$$\delta \Pi^k = 0 \tag{47}$$

The minimization is respect to the unknown coefficients of linear combination introduced in Eq. (35). In particular, Π^k is a function of $U^k_{x\tau_{u_x} i}$, $U^k_{y\tau_{u_y} i}$, $U^k_{z\tau_{u_z} i}$ and the condition given in Eq. (47) can be alternatively written in the following form:

$$\begin{aligned}
&\frac{\partial \Pi^k}{\partial U^k_{x\tau_{u_x} i}} = 0 \quad \text{with} \quad i = 1, \ldots, \mathcal{N}; \quad \tau_{u_x} = b_{u_x}, r_{u_x}, t_{u_x} \quad r_{u_x} = 1, 2, 3, \ldots, N_{u_x} - 1 \\
&\frac{\partial \Pi^k}{\partial U^k_{y\tau_{u_y} i}} = 0 \quad \text{with} \quad i = 1, \ldots, \mathcal{N}; \quad \tau_{u_y} = b_{u_y}, r_{u_y}, t_{u_y} \quad r_{u_y} = 1, 2, 3, \ldots, N_{u_y} - 1 \\
&\frac{\partial \Pi^k}{\partial U^k_{z\tau_{u_z} i}} = 0 \quad \text{with} \quad i = 1, \ldots, \mathcal{N}; \quad \tau_{u_z} = b_{u_z}, b_{u_z}, t_{u_z} \quad r_{u_z} = 1, 2, 3, \ldots, N_{u_z} - 1
\end{aligned} \tag{48}$$

The minimization of the total potential energy of the system leads to the discrete form of the governing differential equations in terms of fundamental primary nuclei:

$$\delta \mathbf{U}^{k^T}_{\tau i} : \quad \left[\mathbf{K}^{k\tau sij} + \lambda_{ij} \mathbf{K}^{k\tau sij}_{\sigma} \right] \mathbf{U}^k_{sj} = 0 \tag{49}$$

The thermal buckling analysis leads to the following eigenvalue problem:

$$\left\| \mathbf{K}^{k\tau sij} + \lambda_{ij} \mathbf{K}^{k\tau sij}_{\sigma} \right\| = 0 \tag{50}$$

and the double bars denote determinant.

THERMAL STABILITY GOVERNING DIFFERENTIAL EQUATIONS

To derive the governing differential equations and natural boundary conditions the Gauss theorem is applied:

$$\begin{aligned}
\int_{\Omega_k} \left(\left(\mathbf{D}_p\right)\,\delta\mathbf{a}^k\right)^T\,\mathbf{a}^k \mathrm{d}\Omega_k &= -\int_{\Omega_k} \delta\mathbf{a}^k\,\left(\left(\mathbf{D}_p\right)^T\,\delta\mathbf{a}^k\right)\,\mathrm{d}\Omega_k + \int_{\Gamma^k} \delta\mathbf{a}^k\,\left(\left(\mathbf{I}_p\right)^T\,\delta\mathbf{a}^k\right)\,\mathrm{d}\Gamma^k \\
\int_{\Omega_k} \left(\left(\mathbf{D}_\Omega\right)\,\delta\mathbf{a}^k\right)^T\,\mathbf{a}^k \mathrm{d}\Omega_k &= -\int_{\Omega_k} \delta\mathbf{a}^k\,\left(\left(\mathbf{D}_\Omega\right)^T\,\delta\mathbf{a}^k\right)\,\mathrm{d}\Omega_k + \int_{\Gamma^k} \delta\mathbf{a}^k\,\left(\left(\mathbf{I}_\Omega\right)^T\,\delta\mathbf{a}^k\right)\,\mathrm{d}\Gamma^k
\end{aligned} \tag{51}$$

where $\mathbf{a}$ can be displacement or stress variables and the introduced $\mathbf{I}_p$ and $\mathbf{I}_\Omega$ arrays are

$$\mathbf{I}_p = \begin{bmatrix} n_x & 0 & 0 \\ 0 & n_y & 0 \\ n_y & n_x & 0 \end{bmatrix}, \quad \mathbf{I}_\Omega = \begin{bmatrix} 0 & 0 & n_x \\ 0 & 0 & n_y \\ 0 & 0 & 0 \end{bmatrix} \tag{52}$$

The normal to the boundary of domain Ω_k is

$$\hat{\mathbf{n}} = \begin{bmatrix} n_x \\ n_y \end{bmatrix} = \begin{bmatrix} \cos\left(\varphi_x\right) \\ \cos\left(\varphi_y\right) \end{bmatrix} \tag{53}$$

where φ_x and φ_y are the direction cosines, namely, the angles between the normal $\hat{\mathbf{n}}$ and the directions x and y, respectively. The governing differential equations and natural boundary conditions (Neumann-type) on Γ_k^m, for a FGM isotropic and sandwich plates at multilayer level can be written as

$$\begin{aligned}
&\sum_{k=1}^{N_l} \int_{\Omega_k} \int_{A^k} \delta\mathbf{u}_\tau \Bigg(- \left[\left(\mathbf{F}_\tau\right)^T\,\left(\mathbf{D}_p\right)^T\right]\left[\widetilde{\mathbf{C}}_{pp}^k \mathbf{D}_p\left(\mathbf{F}_\tau\right) + \widetilde{\mathbf{C}}_{pn}^k \mathbf{D}_{np}\left(\mathbf{F}_\tau\right) + \widetilde{\mathbf{C}}_{pn}^k \mathbf{D}_{nz}\left(\mathbf{F}_\tau\right)\right] \\
&\quad - \left[\left(\mathbf{F}_\tau\right)^T\,\left(\mathbf{D}_{np}\right)^T + \left(\mathbf{F}_\tau\right)^T\,\left(\mathbf{D}_{nz}\right)^T\right]\left[\widetilde{\mathbf{C}}_{np}^k \mathbf{D}_p\left(\mathbf{F}_\tau\right) + \widetilde{\mathbf{C}}_{nn}^k \mathbf{D}_{np}\left(\mathbf{F}_\tau\right) + \widetilde{\mathbf{C}}_{nn}^k \mathbf{D}_{nz}\left(\mathbf{F}_\tau\right)\right]\Bigg) \\
&\quad \times \mathbf{u}_s\, d\Omega_k dz \\
&\quad + \sum_{k=1}^{N_l} \int_{\Gamma_k} \int_{A^k} \delta\mathbf{u}_\tau \Bigg(\left[\left(\mathbf{F}_\tau\right)^T\,\left(\boldsymbol{I}_p\right)^T\right]\left[\widetilde{\mathbf{C}}_{pp}^k \mathbf{D}_p\left(\mathbf{F}_\tau\right) + \widetilde{\mathbf{C}}_{pn}^k \mathbf{D}_{np}\left(\mathbf{F}_\tau\right) + \widetilde{\mathbf{C}}_{pn}^k \mathbf{D}_{nz}\left(\mathbf{F}_\tau\right)\right] \\
&\quad + \left[\left(\mathbf{F}_\tau\right)^T\,\left(\boldsymbol{I}_{np}\right)^T\right]\left[\widetilde{\mathbf{C}}_{np}^k \mathbf{D}_p\left(\mathbf{F}_\tau\right) + \widetilde{\mathbf{C}}_{nn}^k \mathbf{D}_{np}\left(\mathbf{F}_\tau\right) + \widetilde{\mathbf{C}}_{nn}^k \mathbf{D}_{nz}\left(\mathbf{F}_\tau\right)\right]\Bigg) \mathbf{u}_s\, d\Omega_k dz \\
&= \sum_{k=1}^{N_l} \int_{\Omega_k} \int_{A^k} \delta\mathbf{u}_\tau\,\left(\left(\mathbf{F}_\tau\,\mathbf{F}_s\right)^T\,\widetilde{\boldsymbol{\Phi}}\right)\ddot{\mathbf{u}}_s\, d\Omega_k dz
\end{aligned} \tag{54}$$

and in compact form are

$$\begin{aligned}
&\delta\mathbf{u}_\tau: \quad \mathbf{K}^{k\tau s}\,\mathbf{u}_s = \mathbf{K}_\sigma^{k\tau s}\,\mathbf{u}_s \\
&\Gamma_k^m: \quad \boldsymbol{\Pi}^{k\tau s}\,\mathbf{u}_s = \boldsymbol{\Pi}^{k\tau s}\,\bar{\mathbf{u}}_s \quad \Gamma_k^g: \mathbf{u}_s = \bar{\mathbf{u}}_s
\end{aligned} \tag{55}$$

where

$$\mathbf{K}^{k\tau s} = \int_{A^k} \Big(- \left[(\mathbf{F}_\tau)^T \left(\mathbf{D}_p \right)^T \right] \left[\widetilde{\mathbf{C}}^k_{pp} \mathbf{D}_p (\mathbf{F}_\tau) + \widetilde{\mathbf{C}}^k_{pn} \mathbf{D}_{np} (\mathbf{F}_\tau) + \widetilde{\mathbf{C}}^k_{pn} \mathbf{D}_{nz} (\mathbf{F}_\tau) \right] - \left[(\mathbf{F}_\tau)^T \left(\mathbf{D}_{np} \right)^T + (\mathbf{F}_\tau)^T \left(\mathbf{D}_{nz} \right)^T \right] \left[\widetilde{\mathbf{C}}^k_{np} \mathbf{D}_p (\mathbf{F}_\tau) + \widetilde{\mathbf{C}}^k_{nn} \mathbf{D}_{np} (\mathbf{F}_\tau) + \widetilde{\mathbf{C}}^k_{nn} \mathbf{D}_{nz} (\mathbf{F}_\tau) \right] \Big) dz \tag{56}$$

$$\mathbf{\Pi}^{k\tau s} = \int_{A^k} \Big(\left[(\mathbf{F}_\tau)^T \left(\boldsymbol{I}_p \right)^T \right] \left[\widetilde{\mathbf{C}}^k_{pp} \mathbf{D}_p (\mathbf{F}_\tau) + \widetilde{\mathbf{C}}^k_{pn} \mathbf{D}_{np} (\mathbf{F}_\tau) + \widetilde{\mathbf{C}}^k_{pn} \mathbf{D}_{nz} (\mathbf{F}_\tau) \right] \left[(\mathbf{F}_\tau)^T \left(\boldsymbol{I}_{np} \right)^T \right] \left[\widetilde{\mathbf{C}}^k_{np} \mathbf{D}_p (\mathbf{F}_\tau) + \widetilde{\mathbf{C}}^k_{nn} \mathbf{D}_{np} (\mathbf{F}_\tau) + \widetilde{\mathbf{C}}^k_{nn} \mathbf{D}_{nz} (\mathbf{F}_\tau) \right] \Big) dz$$

$$\mathbf{K}^{k\tau s}_\sigma = \int_{A^k} \left((\mathbf{F}_\tau \mathbf{F}_s)^T \, \widetilde{\mathbf{\Phi}} \right) dz$$

The matrix $\widetilde{\mathbf{\Phi}} = \mathrm{diag}\big(\tilde{\Phi}_{11}, \tilde{\Phi}_{22}, \tilde{\Phi}_{33}\big)$, where

$$\begin{cases} \tilde{\Phi}_{11} = \tilde{\sigma}^{\vartheta}_{xx_0} \dfrac{\partial}{\partial x} \dfrac{\partial}{\partial x} + \tilde{\sigma}^{\vartheta}_{yy_0} \dfrac{\partial}{\partial y} \dfrac{\partial}{\partial y} \\ \tilde{\Phi}_{22} = \tilde{\sigma}^{\vartheta}_{xx_0} \dfrac{\partial}{\partial x} \dfrac{\partial}{\partial x} + \tilde{\sigma}^{\vartheta}_{yy_0} \dfrac{\partial}{\partial y} \dfrac{\partial}{\partial y} \\ \tilde{\Phi}_{33} = \tilde{\sigma}^{\vartheta}_{xx_0} \dfrac{\partial}{\partial x} \dfrac{\partial}{\partial x} + \tilde{\sigma}^{\vartheta}_{yy_0} \dfrac{\partial}{\partial y} \dfrac{\partial}{\partial y} \end{cases} \tag{57}$$

The nine components of the fundamental primary differential nucleus $\mathbf{K}$ are given as

$$\begin{aligned} K_{uu}^{k\,\tau_{u_x} s_{u_x}} = & -\widetilde{C}^k_{11} J^{k\tau_{u_x} s_{u_x}} \left(\frac{\partial}{\partial x} \right)_{s_{u_x}} \left(\frac{\partial}{\partial x} \right)_{\tau_{u_x}} - \widetilde{C}^k_{16} J^{k\tau_{u_x} s_{u_x}} \left(\frac{\partial}{\partial x} \right)_{\tau_{u_x}} \left(\frac{\partial}{\partial y} \right)_{s_{u_x}} \\ & - \widetilde{C}^k_{16} J^{k\tau_{u_x} s_{u_x}} \left(\frac{\partial}{\partial x} \right)_{s_{u_x}} \left(\frac{\partial}{\partial y} \right)_{\tau_{u_x}} - \widetilde{C}^k_{66} J^{k\tau_{u_x} s_{u_x}} \left(\frac{\partial}{\partial y} \right)_{s_{u_x}} \left(\frac{\partial}{\partial y} \right)_{\tau_{u_x}} \\ & + \widetilde{C}^k_{55} J^{k\tau_{u_{x_z}} s_{u_{x_z}}} \\ K_{uu}^{k\,\tau_{u_x} s_{u_y}} = & -\widetilde{C}^k_{12} J^{k\tau_{u_x} s_{u_y}} \left(\frac{\partial}{\partial x} \right)_{\tau_{u_x}} \left(\frac{\partial}{\partial y} \right)_{s_{u_y}} - \widetilde{C}^k_{16} J^{k\tau_{u_x} s_{u_y}} \left(\frac{\partial}{\partial x} \right)_{s_{u_x}} \left(\frac{\partial}{\partial x} \right)_{\tau_{u_y}} \\ & - \widetilde{C}^k_{26} J^{k\tau_{u_x} s_{u_y}} \left(\frac{\partial}{\partial y} \right)_{s_{u_y}} \left(\frac{\partial}{\partial y} \right)_{\tau_{u_x}} - \widetilde{C}^k_{66} J^{k\tau_{u_x} s_{u_y}} \left(\frac{\partial}{\partial x} \right)_{s_{u_y}} \left(\frac{\partial}{\partial y} \right)_{\tau_{u_x}} \\ & + \widetilde{C}^k_{45} J^{k\tau_{u_{x_z}} s_{u_{y_z}}} \\ K_{uu}^{k\,\tau_{u_x} s_{u_z}} = & -\widetilde{C}^k_{13} J^{k\tau_{u_x} s_{u_{z_z}}} \left(\frac{\partial}{\partial x} \right)_{\tau_{u_x}} - \widetilde{C}^k_{36} J^{k\tau_{u_x} s_{u_z}} \left(\frac{\partial}{\partial y} \right)_{\tau_{u_x}} + \widetilde{C}^k_{45} J^{k\,\tau_{u_{x_z}} s_{u_z}} \left(\frac{\partial}{\partial y} \right)_{s_{u_z}} \\ & + \widetilde{C}^k_{55} J^{k\,\tau_{u_{x_z}} s_{u_z}} \left(\frac{\partial}{\partial x} \right)_{s_{u_z}} \end{aligned}$$

$$
\begin{aligned}
K_{uu}^{k\,\tau_{u_y}\,s_{u_x}} &= -\widetilde{C}_{12}^{k}\, J^{k\tau_{u_y}s_{u_x}} \left(\frac{\partial}{\partial x}\right)_{s_{u_x}} \left(\frac{\partial}{\partial y}\right)_{\tau_{u_y}} - \widetilde{C}_{16}^{k}\, J^{k\tau_{u_y}s_{u_x}} \left(\frac{\partial}{\partial x}\right)_{s_{u_x}} \left(\frac{\partial}{\partial x}\right)_{\tau_{u_y}} \\
&\quad - \widetilde{C}_{26}^{k}\, J^{k\tau_{u_y}s_{u_x}} \left(\frac{\partial}{\partial y}\right)_{s_{u_x}} \left(\frac{\partial}{\partial y}\right)_{\tau_{u_y}} - \widetilde{C}_{66}^{k}\, J^{k\tau_{u_y}s_{u_x}} \left(\frac{\partial}{\partial x}\right)_{\tau_{u_y}} \left(\frac{\partial}{\partial y}\right)_{s_{u_x}} \\
&\quad + \widetilde{C}_{45}^{k}\, J^{k\tau_{u_{y_z}}s_{u_{x_z}}} \\
K_{uu}^{k\,\tau_{u_y}\,s_{u_y}} &= -\widetilde{C}_{22}^{k}\, J^{k\tau_{u_y}s_{u_y}} \left(\frac{\partial}{\partial x}\right)_{s_{u_y}} \left(\frac{\partial}{\partial x}\right)_{\tau_{u_y}} - \widetilde{C}_{26}^{k}\, J^{k\tau_{u_y}s_{u_y}} \left(\frac{\partial}{\partial x}\right)_{s_{u_y}} \left(\frac{\partial}{\partial y}\right)_{\tau_{u_y}} \\
&\quad - \widetilde{C}_{26}^{k}\, J^{k\tau_{u_y}s_{u_y}} \left(\frac{\partial}{\partial x}\right)_{\tau_{u_y}} \left(\frac{\partial}{\partial y}\right)_{s_{u_y}} - \widetilde{C}_{66}^{k}\, J^{k\tau_{u_y}s_{u_y}} \left(\frac{\partial}{\partial x}\right)_{s_{u_x}} \left(\frac{\partial}{\partial y}\right)_{\tau_{u_y}} \\
&\quad + \widetilde{C}_{44}^{k}\, J^{k\tau_{u_{y_z}}s_{u_{y_z}}} \\
K_{uu}^{k\,\tau_{u_y}\,s_{u_z}} &= -\widetilde{C}_{23}^{k}\, J^{k\tau_{u_y}s_{u_{z_z}}} \left(\frac{\partial}{\partial y}\right)_{\tau_{u_y}} - \widetilde{C}_{36}^{k}\, J^{k\tau_{u_y}s_{u_z}} \left(\frac{\partial}{\partial x}\right)_{\tau_{u_x}} + \widetilde{C}_{45}^{k}\, J^{k\,\tau_{u_{y_z}}s_{u_z}} \left(\frac{\partial}{\partial x}\right)_{s_{u_z}} \\
&\quad + \widetilde{C}_{44}^{k}\, J^{k\,\tau_{u_{y_z}}s_{u_z}} \left(\frac{\partial}{\partial y}\right)_{s_{u_z}} \\
K_{uu}^{k\,\tau_{u_z}\,s_{u_x}} &= +\widetilde{C}_{13}^{k}\, J^{k\tau_{u_{z_z}}s_{u_x}} \left(\frac{\partial}{\partial x}\right)_{s_{u_x}} + \widetilde{C}_{36}^{k}\, J^{k\tau_{u_{z_z}}s_{u_{x_z}}} \left(\frac{\partial}{\partial y}\right)_{s_{u_x}} - \widetilde{C}_{45}^{k}\, J^{k\,\tau_{u_z}s_{u_{x_z}}} \left(\frac{\partial}{\partial y}\right)_{\tau_{u_z}} \\
&\quad - \widetilde{C}_{55}^{k}\, J^{k\,\tau_{u_z}s_{u_{x_z}}} \left(\frac{\partial}{\partial x}\right)_{\tau_{u_z}} \\
K_{uu}^{k\,\tau_{u_z}\,s_{u_y}} &= +\widetilde{C}_{23}^{k}\, J^{k\tau_{u_{z_z}}s_{u_y}} \left(\frac{\partial}{\partial y}\right)_{s_{u_y}} + \widetilde{C}_{36}^{k}\, J^{k\tau_{u_{z_z}}s_{u_y}} \left(\frac{\partial}{\partial x}\right)_{s_{u_y}} - \widetilde{C}_{45}^{k}\, J^{k\,\tau_{u_z}s_{u_{y_z}}} \left(\frac{\partial}{\partial x}\right)_{\tau_{u_z}} \\
&\quad - \widetilde{C}_{44}^{k}\, J^{k\,\tau_{u_z}s_{u_{y_z}}} \left(\frac{\partial}{\partial y}\right)_{\tau_{u_z}} \\
K_{uu}^{k\,\tau_{u_z}\,s_{u_z}} &= \widetilde{C}_{33}^{k}\, J^{k\tau_{u_{z_z}}s_{u_{z_z}}} - \widetilde{C}_{44}^{k}\, J^{k\tau_{u_z}s_{u_z}} \left(\frac{\partial}{\partial y}\right)_{s_{u_z}} \left(\frac{\partial}{\partial y}\right)_{\tau_{u_z}} - \widetilde{C}_{55}^{k}\, J^{k\tau_{u_z}s_{u_z}} \left(\frac{\partial}{\partial x}\right)_{s_{u_z}} \left(\frac{\partial}{\partial x}\right)_{\tau_{u_z}} \\
&\quad - \widetilde{C}_{45}^{k}\, J^{k\tau_{u_z}s_{u_z}} \left(\frac{\partial}{\partial x}\right)_{s_{u_z}} \left(\frac{\partial}{\partial y}\right)_{\tau_{u_z}} - \widetilde{C}_{45}^{k}\, J^{k\tau_{u_z}s_{u_z}} \left(\frac{\partial}{\partial x}\right)_{\tau_{u_z}} \left(\frac{\partial}{\partial y}\right)_{s_{u_z}}
\end{aligned}
\tag{58}
$$

The nine components of the primary fundamental boundary nucleus $\mathbf{\Pi}$ can be written as

$$
\begin{aligned}
\Pi_{uu}^{k\,\tau_{u_x}\,s_{u_x}} &= n_x\, \widetilde{C}_{11}^{k}\, J^{k\tau_{u_x}s_{u_x}} \left(\frac{\partial}{\partial x}\right)_{s_{u_x}} + n_y\, \widetilde{C}_{66}^{k}\, J^{k\tau_{u_x}s_{u_x}} \left(\frac{\partial}{\partial y}\right)_{s_{u_x}} + n_y\, \widetilde{C}_{16}^{k}\, J^{k\tau_{u_x}s_{u_x}} \left(\frac{\partial}{\partial x}\right)_{s_{u_x}} \\
&\quad + n_x\, \widetilde{C}_{16}^{k}\, J^{k\tau_{u_x}s_{u_x}} \left(\frac{\partial}{\partial y}\right)_{s_{u_x}}
\end{aligned}
$$

$$\Pi_{uu}^{k\,\tau_{u_x}s_{u_y}} = n_x\,\widetilde{C}_{16}^{k}\,J^{k\tau_{u_x}s_{u_y}}\left(\frac{\partial}{\partial x}\right)_{s_{u_y}} + n_y\,\widetilde{C}_{26}^{k}\,J^{k\tau_{u_x}s_{u_y}}\left(\frac{\partial}{\partial y}\right)_{s_{u_y}} + n_y\,\widetilde{C}_{66}^{k}\,J^{k\tau_{u_x}s_{u_y}}\left(\frac{\partial}{\partial x}\right)_{s_{u_y}} + n_x\,\widetilde{C}_{12}^{k}\,J^{k\tau_{u_x}s_{u_y}}\left(\frac{\partial}{\partial y}\right)_{s_{u_y}}$$

$$\Pi_{uu}^{k\,\tau_{u_x}s_{u_z}} = n_x\,\widetilde{C}_{13}^{k}\,J^{k\tau_{u_x}s_{u_{z_z}}} + n_y\,\widetilde{C}_{36}^{k}\,J^{k\tau_{u_x}s_{u_{z_z}}}$$

$$\Pi_{uu}^{k\,\tau_{u_y}s_{u_x}} = n_x\,\widetilde{C}_{16}^{k}\,J^{k\tau_{u_y}s_{u_x}}\left(\frac{\partial}{\partial x}\right)_{s_{u_x}} + n_y\,\widetilde{C}_{26}^{k}\,J^{k\tau_{u_y}s_{u_x}}\left(\frac{\partial}{\partial y}\right)_{s_{u_x}} + n_y\,\widetilde{C}_{12}^{k}\,J^{k\tau_{u_y}s_{u_x}}\left(\frac{\partial}{\partial x}\right)_{s_{u_x}} + n_x\,\widetilde{C}_{66}^{k}\,J^{k\tau_{u_y}s_{u_x}}\left(\frac{\partial}{\partial y}\right)_{s_{u_x}} \tag{59}$$

Table 1 Critical temperatures of simply supported (SSSS) square FGM isotropic plates

		ΔT_{cr}				
a/h	Theory	$p=0$	$p=0.5$	$p=1$	$p=2$	$p=5$
50	ES-FEM[44]	70.6998	39.4860	32.2723	28.5288	29.3283
	ED_{444}	68.2055	38.6553	31.6979	28.0962	28.9625
100	ES-FEM[44]	17.7187	9.8946	8.0867	7.1492	7.3515
	ED_{444}	17.0871	9.6821	7.9389	7.0379	7.2594

Table 2 Critical temperature of fully clamped (CCCC) square FGM isotropic plates

		ΔT_{cr}				
a/h	Theory	$p=0$	$p=0.5$	$p=1$	$p=2$	$p=5$
50	ES-FEM[44]	188.2834	105.2699	86.0739	76.0781	78.0599
	ED_{222}	185.8634	105.5901	86.6282	76.7304	78.8096
100	ES-FEM[44]	47.4967	26.5411	21.6980	19.1804	19.7017
	ED_{222}	48.0005	27.2915	22.4017	19.8472	20.3664

Table 3 Material 1

Alumina			
E_c [GPa]	$\alpha_c\left[\frac{1}{C^\circ}\right]$	v_c	$\kappa_c\left[\frac{W}{Mk}\right]$
380	7.4×10^{-6}	0.3	10.4
Aluminum			
E_m [GPa]	$\alpha_m\left[\frac{1}{C^\circ}\right]$	v_m	$\kappa_m\left[\frac{W}{Mk}\right]$
70	23×10^{-6}	0.3	204

$$\Pi_{u\,u}^{k\,\tau_{u_y}\,s_{u_y}} = n_x\,\widetilde{C}_{66}^{k}\,J^{k\tau_{u_y}s_{u_y}}\left(\frac{\partial}{\partial x}\right)_{s_{u_y}} + n_y\,\widetilde{C}_{22}^{k}\,J^{k\tau_{u_y}s_{u_y}}\left(\frac{\partial}{\partial y}\right)_{s_{u_y}} + n_y\,\widetilde{C}_{26}^{k}\,J^{k\tau_{u_y}s_{u_y}}\left(\frac{\partial}{\partial x}\right)_{s_{u_y}} + n_x\,\widetilde{C}_{26}^{k}\,J^{k\tau_{u_y}s_{u_y}}\left(\frac{\partial}{\partial y}\right)_{s_{u_y}}$$

$$\Pi_{u\,u}^{k\,\tau_{u_y}\,s_{u_z}} = n_x\,\widetilde{C}_{36}^{k}\,J^{k\tau_{u_y}s_{u_{z_z}}} + n_y\,\widetilde{C}_{23}^{k}\,J^{k\tau_{u_y}s_{u_{z_z}}}$$

$$\Pi_{u\,u}^{k\,\tau_{u_z}\,s_{u_x}} = n_x\,\widetilde{C}_{55}^{k}\,J^{k\tau_{u_x}s_{u_{x_z}}} + n_y\,\widetilde{C}_{45}^{k}\,J^{k\tau_{u_z}s_{u_{x_z}}}$$

$$\Pi_{u\,u}^{k\,\tau_{u_z}\,s_{u_y}} = n_x\,\widetilde{C}_{45}^{k}\,J^{k\tau_{u_x}s_{u_{y_z}}} + n_y\,\widetilde{C}_{44}^{k}\,J^{k\tau_{u_z}s_{u_y}}$$

Table 4 Critical temperatures of different FGM isotropic square plates under uniform temperature rise

		a/h					
p	Theory	10	20	40	60	80	100
0	CLPT[45]	1709.911	427.477	106.869	47.497	26.717	17.099
	HSDT[45]	1617.484	421.516	106.492	47.424	26.693	17.088
Present plate models	EDZ_{888}	1599.294	420.146	106.404	47.405	26.688	17.087
	EDZ_{333}	1599.322	420.146	106.404	47.410	26.691	17.087
	ED_{999}	1599.293	420.146	106.404	47.405	26.688	17.087
	ED_{444}	1599.294	420.146	106.404	47.405	26.688	17.087
	ED_{222}	1609.305	420.844	106.449	47.414	26.691	17.088
1	CLPT	794.377	198.594	49.648	22.066	12.412	7.943
	HSDT	757.891	196.257	49.500	22.037	12.402	7.939
Present plate models	EDZ_{888}	749.261	195.623	49.461	22.029	12.400	7.939
	EDZ_{333}	749.288	195.625	49.461	22.030	12.401	7.939
	ED_{999}	749.261	195.623	49.460	22.029	12.400	7.939
	ED_{444}	749.265	195.623	49.460	22.029	12.400	7.939
	ED_{222}	752.037	195.814	49.473	22.031	12.401	7.939
5	CLPT	726.571	181.642	45.410	20.182	11.352	7.265
	HSDT	678.926	178.528	45.213	20.144	11.340	7.260
Present plate models	EDZ_{888}	669.396	177.803	45.166	20.135	11.339	7.256
	EDZ_{333}	669.817	177.833	45.167	20.135	11.337	7.262
	ED_{999}	669.396	177.803	45.166	20.134	11.337	7.259
	ED_{444}	669.545	177.814	45.167	20.134	11.337	7.259
	ED_{222}	677.859	178.404	45.205	20.142	11.340	7.260
10	CLPT	746.927	186.731	46.682	20.747	11.670	7.469
	HSDT	692.519	183.141	46.455	20.703	11.657	7.462
Present plate models	EDZ_{888}	683.199	182.428	46.408	20.693	11.654	7.460
	EDZ_{333}	683.457	182.445	46.409	20.693	11.652	7.461
	ED_{999}	683.196	182.428	46.408	20.693	11.653	7.462
	ED_{444}	683.368	182.440	46.408	20.693	11.653	7.462
	ED_{222}	694.277	183.220	46.459	20.703	11.656	7.463

$$\Pi_{uu}^{k\,\tau_{u_z}\,s_{u_z}} = n_x\,\widetilde{C}_{55}^{k}\,J^{k\tau_{u_z}s_{u_z}}\left(\frac{\partial}{\partial x}\right)_{s_{u_z}} + n_y\,\widetilde{C}_{44}^{k}\,J^{k\tau_{u_z}s_{u_z}}\left(\frac{\partial}{\partial y}\right)_{s_{u_z}} + n_y\,\widetilde{C}_{45}^{k}\,J^{k\tau_{u_z}s_{u_z}}\left(\frac{\partial}{\partial x}\right)_{s_{u_z}} + n_x\,\widetilde{C}_{45}^{k}\,J^{k\tau_{u_z}s_{u_z}}\left(\frac{\partial}{\partial y}\right)_{s_{u_z}}$$

The three components of the fundamental primary differential initial stress nucleus $\mathbf{K}_{\sigma}^{k\tau s}$ are following reported:

$$K_{\sigma_{uu}}^{k\,\tau_{u_x}\,s_{u_x}} = J^{k\tau_{u_x}s_{u_x}}\left[\tilde{\sigma}_{xx_0}^{\vartheta}\,\frac{\partial}{\partial x}\,\frac{\partial}{\partial x} + \tilde{\sigma}_{yy_0}^{\vartheta}\,\frac{\partial}{\partial y}\,\frac{\partial}{\partial y}\right]$$

$$K_{\sigma_{uu}}^{k\,\tau_{u_y}\,s_{u_y}} = J^{k\tau_{u_y}s_{u_y}}\left[\tilde{\sigma}_{xx_0}^{\vartheta}\,\frac{\partial}{\partial x}\,\frac{\partial}{\partial x} + \tilde{\sigma}_{yy_0}^{\vartheta}\,\frac{\partial}{\partial y}\,\frac{\partial}{\partial y}\right] \tag{60}$$

Table 5 Critical temperatures of different FGM isotropic square plates under linear temperature rise

		a/h					
p	Theory	10	20	40	60	80	100
0	CLPT[45]	3409.821	844.955	203.738	84.995	43.434	24.198
	HSDT[45]	3224.968	833.032	202.984	84.848	43.387	24.177
Present plate models	EDZ_{888}	3188.250	830.287	202.808	84.812	43.377	24.172
	EDZ_{333}	3188.308	830.287	202.808	84.810	43.375	24.172
	ED_{999}	3188.250	830.286	202.808	84.811	43.376	24.174
	ED_{444}	3188.250	830.286	202.808	84.811	43.376	24.174
	ED_{222}	3208.314	831.684	202.898	84.829	43.382	24.177
1	CLPT	1480.450	363.079	83.736	32.006	13.901	5.520
	HSDT	1412.023	358.696	83.459	31.952	13.882	5.513
Present plate models	EDZ_{888}	1399.442	357.768	83.400	31.940	13.880	5.512
	EDZ_{333}	1399.495	357.771	83.399	31.940	13.881	5.513
	ED_{999}	1399.442	357.768	83.400	31.940	13.880	5.512
	ED_{444}	1399.450	357.768	83.400	31.940	13.880	5.512
	ED_{222}	1404.683	358.127	83.423	31.944	13.881	5.513
5	CLPT	1242.035	304.054	69.558	26.133	10.934	3.899
	HSDT	1160.024	298.693	69.219	26.067	10.913	3.891
Present plate models	EDZ_{888}	1147.338	297.737	69.155	26.053	10.909	3.889
	EDZ_{333}	1148.089	297.789	69.158	26.053	10.908	3.892
	ED_{999}	1147.337	297.737	69.155	26.053	10.909	3.889
	ED_{444}	1147.595	297.756	69.156	26.053	10.909	3.889
	ED_{222}	1162.138	298.776	69.222	26.066	10.913	3.891
10	CLPT	1314.743	322.040	73.864	27.906	11.820	4.375
	HSDT	1218.328	315.677	73.461	27.826	11.797	4.364
Present plate models	EDZ_{888}	1204.948	314.663	73.392	27.811	11.791	4.363
	EDZ_{333}	1205.388	314.693	73.394	27.811	11.790	4.361
	ED_{999}	1204.943	314.663	73.392	27.812	11.791	4.363
	ED_{444}	1205.248	314.685	73.394	27.812	11.791	4.363
	ED_{222}	1224.778	316.071	73.483	27.830	11.796	4.365

$$K^{k\,\tau_{u_z}\,s_{u_z}}_{\sigma_{u\,u}} = J^{k\tau_{u_z}s_{u_z}}\left[\tilde{\sigma}^{\vartheta}_{xx_0}\frac{\partial}{\partial x}\frac{\partial}{\partial x} + \tilde{\sigma}^{\vartheta}_{yy_0}\frac{\partial}{\partial y}\frac{\partial}{\partial y}\right]$$

NUMERICAL RESULTS AND DISCUSSION

The Ritz functions in Eq. (41) are chosen to satisfy the simply supported and fully clamped boundary conditions, respectively:

$$\psi^{SS}_{x_{mn}}(x,y) = \sum_m\sum_n \cos\left(\frac{m\,\pi\,x}{a}\right)\,\sin\left(\frac{n\,\pi\,y}{b}\right)$$

$$\psi^{C}_{x_{mn}}(x,y) = \sum_m\sum_n \sin\left(\frac{m\,\pi\,x}{a}\right)\,\sin\left(\frac{n\,\pi\,y}{b}\right)$$

$$\psi^{SS}_{y_{mn}}(x,y) = \sum_m\sum_n \sin\left(\frac{m\,\pi\,x}{a}\right)\,\cos\left(\frac{n\,\pi\,y}{b}\right)$$

Table 6 Critical temperatures of different FGM isotropic square plates under non-linear Fourier temperature rise

		a/h					
p	Theory	10	20	40	60	80	100
0	CLPT[45]	3409.821	844.955	203.738	84.995	43.434	24.198
	HSDT[45]	3224.968	833.032	202.984	84.848	43.387	24.177
Present plate models	EDZ_{888}	3188.250	830.286	202.808	84.811	43.371	24.172
	EDZ_{333}	3188.308	830.287	202.808	84.810	43.375	24.172
	ED_{999}	3188.250	830.286	202.808	84.811	43.376	24.174
	ED_{444}	3188.250	830.286	202.808	84.811	43.376	24.174
	ED_{222}	3208.314	831.684	202.898	84.829	43.382	24.177
1	CLPT	2055.001	503.987	116.234	44.428	19.296	7.663
	HSDT	1960.018	497.903	115.849	44.352	19.270	7.652
Present plate models	EDZ_{888}	1942.064	496.586	115.765	44.335	19.266	7.651
	EDZ_{333}	1942.143	496.590	115.765	44.337	19.269	7.654
	ED_{999}	1942.065	496.586	115.765	44.335	19.266	7.651
	ED_{444}	1942.075	496.587	115.765	44.335	19.266	7.651
	ED_{222}	1949.370	497.085	115.797	44.341	19.268	7.652
5	CLPT	1553.336	380.261	86.999	32.683	13.675	4.877
	HSDT	1450.769	373.557	86.568	32.600	13.648	4.866
Present plate models	EDZ_{888}	1434.646	372.345	86.487	32.582	13.643	4.864
	EDZ_{333}	1435.591	372.411	86.491	32.584	13.643	4.871
	ED_{999}	1434.646	372.345	86.487	32.583	13.643	4.864
	ED_{444}	1434.969	372.369	86.488	32.582	13.643	4.864
	ED_{222}	1453.172	373.645	86.571	32.599	13.648	4.866
10	CLPT	1519.568	372.211	85.372	32.254	13.662	5.057
	HSDT	1408.132	364.857	84.905	32.162	13.634	5.044
Present plate models	EDZ_{888}	1392.477	363.672	84.825	32.144	13.627	5.042
	EDZ_{333}	1392.989	363.707	84.827	32.144	13.628	5.043
	ED_{999}	1392.473	363.672	84.825	32.145	13.627	5.043
	ED_{444}	1392.825	363.698	84.827	32.145	13.628	5.043
	ED_{222}	1415.401	365.300	84.931	32.165	13.634	5.045

$$\psi^{C}_{y_{mn}}(x, y) = \sum_m \sum_n \sin\left(\frac{m\,\pi\,x}{a}\right)\ \sin\left(\frac{n\,\pi\,y}{b}\right) \tag{61}$$

$$\psi^{SS}_{z_{mn}}(x, y) = \sum_m \sum_n \sin\left(\frac{m\,\pi\,x}{a}\right)\ \sin\left(\frac{n\,\pi\,y}{b}\right)$$

$$\psi^{C}_{z_{mn}}(x, y) = \sum_m \sum_n \sin\left(\frac{m\,\pi\,x}{a}\right)\ \sin\left(\frac{n\,\pi\,y}{b}\right)$$

Table 7 Critical temperatures of different FGM isotropic square plates under several non-linear temperature rises and using the ED_{444} kinematics model

		a/h					
p	Theory	10	20	40	60	80	100
0	$\chi = 2$	4773.881	1244.855	304.177	127.210	65.063	36.261
	$\chi = 3$	6354.050	1659.044	405.523	169.604	86.748	48.347
	$\chi = 4$	7930.729	2072.991	506.853	211.996	108.433	60.433
	$\chi = 5$	9505.089	2486.778	608.175	254.386	130.117	72.517
	Fourier	3188.250	830.286	202.808	84.811	43.376	24.174
	Sinusoidal	4380.916	1142.044	279.033	116.692	59.683	33.263
1	$\chi = 2$	2086.412	533.415	124.344	47.620	20.694	8.218
	$\chi = 3$	2797.880	715.644	166.842	63.897	27.767	11.027
	$\chi = 4$	3526.619	902.533	210.442	80.597	35.025	13.910
	$\chi = 5$	4267.737	1092.772	254.834	97.601	42.415	16.844
	Fourier	1942.075	496.587	115.765	44.335	19.266	7.651
	Sinusoidal	1910.606	488.409	113.849	43.600	18.947	7.524
5	$\chi = 2$	1578.690	409.571	95.120	35.834	15.004	5.349
	$\chi = 3$	1993.152	517.248	120.135	45.258	18.950	6.756
	$\chi = 4$	2403.480	623.951	144.930	54.600	22.862	8.151
	$\chi = 5$	2814.801	730.979	169.805	63.972	26.787	9.550
	Fourier	1434.969	372.369	86.488	32.582	13.643	4.864
	Sinusoidal	1465.910	380.280	88.316	33.270	13.931	4.967
10	$\chi = 2$	1658.214	433.043	100.100	38.273	16.226	6.004
	$\chi = 3$	2072.792	541.569	126.326	47.872	20.295	7.510
	$\chi = 4$	2466.180	644.653	150.390	56.992	24.162	8.941
	$\chi = 5$	2847.556	744.649	173.736	65.840	27.913	10.330
	Fourier	1392.825	363.698	84.827	32.145	13.628	5.043
	Sinusoidal	1544.676	403.339	94.069	35.647	15.112	5.592

Table 8 Material 2

$Zr0_2$		
E_c [GPa]	$\alpha_c \left[\frac{1}{C^\circ}\right]$	ν_c
244.27	12.766×10^{-6}	0.3
Ti 6Al 4V		
E_m [GPa]	$\alpha_m \left[\frac{1}{C^\circ}\right]$	ν_m
66.2	10.3×10^{-6}	0.3

Different FGM isotropic and sandwich plates were investigated. The results are given using the usual acronym system used in the CUF [32, 41]. Therefore, the ESL theories are indicated as $ED_{N_{u_\alpha}N_{u_\beta}N_{u_z}}$ where E means the equivalent single layer approach, D means that the Principle of Virtual Displacements has been employed and N_{u_α}, N_{u_β}, N_{u_z} are the three expansion orders used in the displacement field. Similarly, the acronym used to describe the ZZ theories is $EDZ_{N_{u_\alpha}N_{u_\beta}N_{u_z}}$, where Z states that *MZZF* has been introduced.

Thermal Buckling of FGM Plates

A preliminary validation of the developed theories is shown in Tables 1 and 2. In particular, the material used is the Aluminum/Alumina, which properties are

Table 9 Critical temperatures $T_{cr} = 10^{-3}\,\Delta T_{cr}$ of different sandwich square plates under uniform temperature rise and volume fraction index $p = 0.5$

		a/h				
Lamination scheme	Theory	5	10	15	25	50
$1-0-1$	SPT[21]	2.87276	0.80328	0.36504	0.13294	0.03340
	HPT[21]	2.87073	0.80313	0.36501	0.13294	0.03340
	FPT[21]	2.83506	0.80036	0.36444	0.13286	0.03339
Present plate models	EDZ_{888}	2.78102	0.79510	0.36332	0.13272	0.03339
	EDZ_{333}	2.78167	0.79568	0.36485	0.12938	0.03340
	ED_{999}	2.78100	0.79510	0.36332	0.13272	0.03339
	ED_{444}	2.78149	0.79514	0.36332	0.13272	0.03339
	ED_{111}	3.34160	0.96851	0.44391	0.16243	0.04089
$2-1-2$	SPT	2.83194	0.79232	0.36010	0.13116	0.03295
	HPT	2.83029	0.79220	0.36007	0.13115	0.03295
	FPT	2.79675	0.78959	0.35954	0.13108	0.03295
Present plate models	EDZ_{888}	2.74262	0.78433	0.35841	0.13093	0.03294
	EDZ_{333}	2.74299	0.78434	0.35842	0.13093	0.03294
	ED_{999}	2.74262	0.78433	0.35841	0.13093	0.03294
	ED_{444}	2.74280	0.78434	0.35842	0.13093	0.03294
	ED_{111}	3.29644	0.95547	0.43793	0.16024	0.04034
$1-1-1$	SPT	2.83331	0.79463	0.36134	0.13164	0.03308
	HPT	2.83224	0.79456	0.36132	0.13164	0.03308
	FPT	2.80230	0.79223	0.36084	0.13157	0.03307
Present plate models	EDZ_{888}	2.74476	0.78663	0.35964	0.13142	0.03307
	EDZ_{333}	2.74503	0.78664	0.35964	0.13142	0.03307
	ED_{999}	2.74473	0.78663	0.35964	0.13142	0.03307
	ED_{444}	2.74482	0.78663	0.35964	0.13142	0.03307
	ED_{111}	3.30155	0.95848	0.43948	0.16084	0.04050
$1-2-1$	SPT	2.86992	0.80925	0.36841	0.13430	0.03376
	HPT	2.86971	0.80925	0.36841	0.13430	0.03376
	FPT	2.84659	0.80745	0.36804	0.13425	0.03375
Present plate models	EDZ_{888}	2.78032	0.80099	0.36665	0.13407	0.03374
	EDZ_{333}	2.78085	0.80102	0.36666	0.13407	0.03374
	ED_{999}	2.78032	0.80099	0.36665	0.13407	0.03374
	ED_{444}	2.78057	0.80101	0.36666	0.13407	0.03374
	ED_{111}	3.35012	0.97647	0.44815	0.16410	0.04132

given in Table 3. In Tables 1 and 2, results for simply supported and fully clamped boundary conditions are compared against those proposed by Nguyen-Xuan et al. [44] using the edge-smoothed finite element method. As can be seen the results in terms of critical temperature for different values of the volume fraction index are in excellent agreement, for both the boundary conditions taken into account. Two different thickness-to-length ratios were examined: $a/h = 50$ and $a/h = 100$. As can be observed the critical temperature decreases both when increasing the volume fraction index (p) and when increasing the thickness-to-length ratio (a/h). As expected the fully clamped (CCCC) boundary condition leads to higher critical temperatures than those computed using the simply supported (SSSS) one. In the

Table 10 Critical temperatures $T_{cr} = 10^{-3}\,\Delta T_{cr}$ of different sandwich square plates under uniform temperature rise and volume fraction index $p = 2$

		a/h				
Lamination scheme	Theory	5	10	15	25	50
$1-0-1$	SPT[21]	2.63459	0.71815	0.32462	0.11789	0.02958
	HPT[21]	2.63018	0.71783	0.32455	0.11788	0.02958
	FPT[21]	2.57355	0.71357	0.32368	0.11776	0.02957
Present plate models	EDZ_{888}	2.53838	0.71029	0.32298	0.11768	0.02957
	EDZ_{333}	2.54581	0.71088	0.32311	0.11770	0.02960
	ED_{999}	2.53828	0.71028	0.32298	0.11768	0.02957
	ED_{444}	2.54580	0.71088	0.32311	0.11769	0.02957
	ED_{111}	3.04976	0.86525	0.39464	0.14402	0.03621
$2-1-2$	SPT	2.39953	0.65098	0.29396	0.10671	0.02677
	HPT	2.39637	0.65075	0.29392	0.10670	0.02676
	FPT	2.34733	0.64710	0.29317	0.10660	0.02676
Present plate models	EDZ_{888}	2.32049	0.64461	0.29265	0.10653	0.02676
	EDZ_{333}	2.32393	0.64488	0.29270	0.10654	0.02676
	ED_{999}	2.32049	0.64461	0.29265	0.10653	0.02676
	ED_{444}	2.32393	0.64488	0.29270	0.10654	0.02676
	ED_{111}	2.78709	0.78520	0.35757	0.13038	0.03277
$1-1-1$	SPT	2.36195	0.64253	0.29031	0.10541	0.02645
	HPT	2.35999	0.64238	0.29028	0.10540	0.02645
	FPT	2.31737	0.63921	0.28963	0.10532	0.02644
Present plate models	EDZ_{888}	2.29107	0.63675	0.28911	0.10525	0.02644
	EDZ_{333}	2.29231	0.63684	0.28913	0.10525	0.02644
	ED_{999}	2.29075	0.63672	0.28911	0.10525	0.02644
	ED_{444}	2.29229	0.63684	0.28913	0.10525	0.02644
	ED_{111}	2.75073	0.77555	0.35323	0.12881	0.03237
$1-2-1$	SPT	2.42899	0.66689	0.30189	0.10972	0.02754
	HPT	2.42873	0.66687	0.30189	0.10972	0.02754
	FPT	2.39541	0.66436	0.30138	0.10966	0.02754
Present plate models	EDZ_{888}	2.35962	0.66102	0.30066	0.10956	0.02753
	EDZ_{333}	2.36129	0.66116	0.30069	0.10956	0.02753
	ED_{999}	2.35962	0.66102	0.30066	0.10956	0.02753
	ED_{444}	2.36123	0.66115	0.30069	0.10956	0.02753
	ED_{111}	2.83790	0.80550	0.36743	0.13409	0.03372

case of CCCC boundary condition the convergence has been reached by using $M = N = 16$ as half-wave numbers.

In Table 4 a deep assessment of the developed ESL and ZZ plate theories is carried out comparing the results with the analytical solutions based on a CLPT and a HSDT, provided by Javaheri and Eslami [45]. The proposed results represent the critical temperature of Aluminum/Aluminia FGM isotropic plates (Material 1, see Table 3), when subjected under a uniform temperature rise through-the-thickness direction.

Results match very well from moderately thick ($a/h = 10$) to thin ($a/h = 100$) FGM isotropic plates. The proposed higher-order ESL and ZZ theories using a higher number of degrees of freedom (DOFs) lead to more refined results. It is

Table 11 Critical temperatures $T_{cr} = 10^{-3}\,\Delta T_{cr}$ of different sandwich square plates under linear temperature rise ($\chi = 1$) and volume fraction index $p = 0.5$

		a/h				
Lamination scheme	Theory	5	10	15	25	50
$1-0-1$	SPT[21]	5.69553	1.55657	0.68008	0.21589	0.01680
	HPT[21]	5.69147	1.55627	0.68002	0.21588	0.01680
	FPT[21]	5.62013	1.55073	0.67888	0.21573	0.01679
Present plate models	EDZ_{888}	5.50856	1.54014	0.67663	0.21544	0.01678
	EDZ_{333}	5.50992	1.54022	0.67664	0.21544	0.01678
	ED_{999}	5.50852	1.54013	0.67663	0.21544	0.01678
	ED_{444}	5.50951	1.54021	0.67664	0.21544	0.01678
	ED_{111}	6.62896	1.88692	0.83780	0.27485	0.03178
$2-1-2$	SPT	5.61388	1.53464	0.67020	0.21231	0.01590
	HPT	5.61059	1.53440	0.67015	0.21231	0.01590
	FPT	5.54350	1.52919	0.66908	0.21216	0.01589
Present plate models	EDZ_{888}	5.43183	1.51858	0.66682	0.21186	0.01587
	EDZ_{333}	5.43261	1.51862	0.66683	0.21187	0.01588
	ED_{999}	5.43183	1.51858	0.66682	0.21186	0.01588
	ED_{444}	5.43220	1.51861	0.66682	0.21187	0.01588
	ED_{111}	6.53874	1.86084	0.82586	0.27048	0.03068
$1-1-1$	SPT	5.61662	1.53926	0.67268	0.21329	0.01615
	HPT	5.61448	1.53912	0.67265	0.21328	0.01615
	FPT	5.55460	1.53446	0.67169	0.21315	0.01614
Present plate models	EDZ_{888}	5.43604	1.52318	0.66928	0.21283	0.01613
	EDZ_{333}	5.43663	1.52320	0.66928	0.21283	0.01613
	ED_{999}	5.43599	1.52318	0.66928	0.21283	0.01613
	ED_{444}	5.43616	1.52319	0.66928	0.21283	0.01613
	ED_{111}	6.54888	1.86687	0.82895	0.27168	0.03099
$1-2-1$	SPT	5.68984	1.56851	0.68682	0.21860	0.01751
	HPT	5.68943	1.56850	0.68682	0.21860	0.01751
	FPT	5.64318	1.56490	0.68608	0.21850	0.01750
Present plate models	EDZ_{888}	5.50698	1.55190	0.68329	0.21813	0.01748
	EDZ_{333}	5.50808	1.55196	0.68331	0.21813	0.01748
	ED_{999}	5.50698	1.55190	0.68329	0.21813	0.01748
	ED_{444}	5.50748	1.55194	0.68330	0.21813	0.01748
	ED_{111}	6.64582	1.90283	0.84629	0.27819	0.03265

interesting to note that the proposed ED_{222} plate model, especially for thin FGM isotropic plates, leads to exactly the same results of the HSDT given by Javaheri and Eslami [45]. The trends of the critical temperature, as already observed in Tables 1 and 2, decreases when increasing both the volume fraction index and the thickness-to-length ratio.

In Tables 5 and 6, the critical temperatures are computed accounting for a linear and a non-linear temperature rise through-the-thickness of the FGM isotropic plate, respectively, and considering $T_m = 5°C$.

As can be seen in Tables 5 and 6, the critical temperatures of a FGM isotropic plate, when subjected to a linear temperature distribution through-the-thickness, are higher than those evaluated considering a uniform temperature rise

Table 12 Critical temperatures $T_{cr} = 10^{-3}\,\Delta T_{cr}$ of different sandwich square plates under linear temperature rise ($\chi = 1$) and volume fraction index $p = 2$

		a/h				
Lamination scheme	Theory	5	10	15	25	50
$1-0-1$	SPT[21]	5.21919	1.38631	0.59924	0.18578	0.00916
	HPT[21]	5.21036	1.38566	0.59911	0.18576	0.00917
	FPT[21]	5.09710	1.37714	0.59736	0.18553	0.00915
Present plate models	EDZ_{888}	5.02496	1.37054	0.59596	0.18535	0.00914
	EDZ_{333}	5.03986	1.37172	0.59621	0.18538	0.00921
	ED_{999}	5.02475	1.37052	0.59596	0.18535	0.00914
	ED_{444}	5.03982	1.37172	0.59621	0.18538	0.00914
	ED_{111}	6.04724	1.68045	0.73928	0.23803	0.02243
$2-1-2$	SPT	4.74906	1.25196	0.53793	0.16341	0.00354
	HPT	4.74274	1.25150	0.53784	0.16340	0.00354
	FPT	4.64467	1.24420	0.53635	0.16320	0.00353
Present plate models	EDZ_{888}	4.58978	1.23919	0.53529	0.16306	0.00352
	EDZ_{333}	4.59657	1.23972	0.53540	0.16308	0.00352
	ED_{999}	4.58966	1.23919	0.53529	0.16306	0.00352
	ED_{444}	4.59654	1.23973	0.53540	0.16308	0.00352
	ED_{111}	5.52250	1.52037	0.66513	0.21075	0.01554
$1-1-1$	SPT	4.67391	1.23506	0.53063	0.16082	0.00289
	HPT	4.66999	1.23477	0.53057	0.16081	0.00289
	FPT	4.58474	1.22842	0.52927	0.16064	0.00288
Present plate models	EDZ_{888}	4.53086	1.22347	0.52822	0.16050	0.00288
	EDZ_{333}	4.53336	1.22366	0.52826	0.16051	0.00288
	ED_{999}	4.53023	1.22342	0.52821	0.16050	0.00288
	ED_{444}	4.53331	1.22366	0.52826	0.16051	0.00288
	ED_{111}	5.44983	1.50107	0.65646	0.20761	0.01476
$1-2-1$	SPT	4.80799	1.28377	0.55379	0.16944	0.00508
	HPT	4.80746	1.28375	0.55378	0.16944	0.00508
	FPT	4.74083	1.27872	0.55275	0.16931	0.00507
Present plate models	EDZ_{888}	4.66775	1.27202	0.55133	0.16912	0.00506
	EDZ_{333}	4.67111	1.27228	0.55137	0.16913	0.00506
	ED_{999}	4.66775	1.27202	0.55133	0.16912	0.00506
	ED_{444}	4.67097	1.27228	0.55138	0.16913	0.00507
	ED_{111}	5.62392	1.56096	0.68485	0.21819	0.01744

through-the-thickness but lower than those computed when accounting for a non-linear temperature distribution through-the-thickness. In Table 6, the non-linear temperature rise through-the-thickness is computed by solving the one-dimensional Fourier heat conduction equation.

In Table 7, the critical temperatures of FGM plates are evaluated accounting for several non-linear temperature rises through-the-thickness. Most notably, when the temperature rise through-the-thickness is considered functionally graded, then the critical temperature increases when increasing the temperature index χ, for example in Table 7, $\chi = 2, 3, 4, 5$. The lower critical temperature is obtained when considering the Fourier non-linear temperature distribution. Tacking into account the sinusoidal temperature distribution, the critical temperature is comparable to the

Table 13 Critical temperatures $T_{cr} = 10^{-3}\,\Delta T_{cr}$ of different sandwich square plates under non-linear temperature rise ($\chi = 5$) and volume fraction index $p = 0.5$

		a/h				
Lamination scheme	Theory	5	10	15	25	50
$1-0-1$	SPT[21]	21.62877	5.91108	2.58262	0.81985	0.06380
	HPT[21]	21.61337	5.90995	2.58239	0.81982	0.06380
	FPT[21]	21.34245	5.88890	2.57804	0.81924	0.06376
Present plate models	EDZ_{888}	20.48376	5.81323	2.56225	0.81725	0.06369
	EDZ_{333}	20.49316	5.81362	2.56232	0.81725	0.06369
	ED_{999}	20.48360	5.81321	2.56225	0.81725	0.06369
	ED_{444}	20.48612	5.81348	2.56231	0.81726	0.06369
	ED_{111}	24.32680	7.09122	3.16612	1.04185	0.12062
$2-1-2$	SPT	21.35073	5.83656	2.54893	0.80746	0.06048
	HPT	21.33821	5.83566	2.54875	0.80744	0.06048
	FPT	21.08306	5.81584	2.54466	0.80689	0.06044
Present plate models	EDZ_{888}	20.27537	5.75306	2.53437	0.80661	0.06053
	EDZ_{333}	20.28301	5.75328	2.53440	0.80663	0.06050
	ED_{999}	20.27537	5.75306	2.53437	0.80663	0.06054
	ED_{444}	20.27610	5.75315	2.53439	0.80663	0.06050
	ED_{111}	24.09096	7.01939	3.13249	1.02904	0.11688
$1-1-1$	SPT	21.13243	5.79146	2.53095	0.80248	0.06078
	HPT	21.12437	5.79091	2.53084	0.80247	0.06078
	FPT	20.89907	5.77339	2.52722	0.80199	0.06075
Present plate models	EDZ_{888}	20.23122	5.75312	2.53600	0.80784	0.06120
	EDZ_{333}	20.23894	5.75329	2.53603	0.80786	0.06127
	ED_{999}	20.23102	5.75309	2.53600	0.80786	0.06121
	ED_{444}	20.23183	5.75315	2.53601	0.80785	0.06127
	ED_{111}	24.06194	7.02122	3.13474	1.03046	0.11770
$1-2-1$	SPT	20.80527	5.73535	2.51143	0.79933	0.06402
	HPT	20.80375	5.73532	2.51144	0.79933	0.06402
	FPT	20.63465	5.72216	2.50871	0.79897	0.06400
Present plate models	EDZ_{888}	20.41141	5.83674	2.57804	0.82440	0.06612
	EDZ_{333}	20.42205	5.83710	2.57804	0.82440	0.06612
	ED_{999}	20.41140	5.83675	2.57803	0.82440	0.06612
	ED_{444}	20.41447	5.83694	2.57807	0.82440	0.06612
	ED_{111}	24.32828	7.12676	3.18670	1.05062	0.12345

one obtained using $\chi = 2$. This is quite understandable; indeed looking at Figure 4 the two temperature distributions are similar.

Thermal Buckling of FGM Sandwich Plates

Several FGM sandwich plates made up of $Zr0_2$/Ti 6Al 4V (Material 2, see Table 8), from Table 9 to Table 14, are examined. In particular, different FGM sandwich plate configurations, which are depicted in Figure 3, are subjected to various temperature distributions through-the-thickness direction. The FGM sandwich plates are composed of FGM face sheets and a ceramic core (see Figure 1b). In the present investigation for the linear and non-linear temperature

Table 14 Critical temperatures $T_{cr} = 10^{-3}\,\Delta T_{cr}$ of different sandwich square plates under non-linear temperature rise ($\chi = 5$) and volume fraction index $p = 2$

		a/h				
Lamination scheme	Theory	5	10	15	25	50
$1-0-1$	SPT[21]	23.06830	6.12734	2.64858	0.82115	0.04051
	HPT[21]	23.02926	6.12449	2.64800	0.82107	0.04052
	FPT[21]	22.52869	6.08684	2.64029	0.82005	0.04044
Present plate models	EDZ_{888}	21.70772	6.01748	2.62604	0.81831	0.04040
	EDZ_{333}	21.76775	6.02255	2.62712	0.81847	0.04028
	ED_{999}	21.70677	6.01741	2.62603	0.81831	0.04038
	ED_{444}	21.76380	6.02248	2.62711	0.81845	0.04039
	ED_{111}	25.71472	7.34202	3.25013	1.05003	0.09908
$2-1-2$	SPT	22.38252	5.90053	2.53532	0.77017	0.01668
	HPT	22.35275	5.89838	2.53488	0.77011	0.01668
	FPT	21.89054	5.86398	2.52785	0.76918	0.01662
Present plate models	EDZ_{888}	21.24283	5.82465	2.52460	0.77048	0.01639
	EDZ_{333}	21.27146	5.82705	2.52511	0.77052	0.01664
	ED_{999}	21.24229	5.82461	2.52460	0.77045	0.01664
	ED_{444}	21.26902	5.82701	2.52511	0.77052	0.01664
	ED_{111}	25.17843	7.11324	3.13025	0.99501	0.07349
$1-1-1$	SPT	22.00152	5.81379	2.49783	0.75703	0.01363
	HPT	21.98303	5.81247	2.49756	0.75699	0.01363
	FPT	21.58175	5.78254	2.49144	0.75619	0.01358
Present plate models	EDZ_{888}	21.22219	5.81520	2.51878	0.76668	0.01375
	EDZ_{333}	21.23387	5.81632	2.51897	0.76667	0.01375
	ED_{999}	21.21930	5.81520	2.51873	0.76668	0.01375
	ED_{444}	21.23175	5.81629	2.51896	0.76667	0.01375
	ED_{111}	25.17488	7.10418		0.99097	0.07054
$1-2-1$	SPT	21.54917	5.75380	2.48205	0.75946	0.02279
	HPT	21.54679	5.75368	2.48202	0.75946	0.02279
	FPT	21.24818	5.73116	2.47740	0.75885	0.02275
Present plate models	EDZ_{888}	21.56980	5.95798	2.58983	0.79567	0.02384
	EDZ_{333}	21.58801	5.95927	2.59009	0.79570	0.02385
	ED_{999}	21.56978	5.95798	2.58983	0.79567	0.02384
	ED_{444}	21.58557	5.95922	2.59009	0.79570	0.02385
	ED_{111}	25.67606	7.28319	3.21127	1.02583	0.08209

rises, $T_t = 25°C$. Results, in terms of critical buckling temperatures, were compared with those proposed by Zenkour and Sobhy [21]. In particular, the latter were obtained by using first-order shear deformation plate theory (FPT), higher-order shear deformation plate theory (HPT) and sinusoidal shear deformation plate theory (SDT). In Tables 9 and 10 the critical temperatures were computed for different values of the thickness-to-length ratio and different values of the volume fraction index. More specifically, for $p = 0.5$ in Table 9 and $p = 2$ in Table 10, the temperature rise through-the-thickness is considered uniform. As expected, independently of the values assumed by the volume fraction index, the critical temperature decreases when increasing the thickness-to-length ratio. The highest critical temperature is reached with the FGM sandwich plate configuration 1-0-1 (see Figure 3a). The same analysis was carried out in Tables 11 and 12 considering a linear temperature distribution through-the-thickness and in Tables 13 and 14 taking into account a non-linear temperature distribution ($\chi = 5$) (see Figure 4). It is interesting to note that for uniform and linear temperature rises through-the-thickness the critical temperatures computed with $p = 0.5$ are higher than those computed with $p = 2$. In sharp contrast, when a non-linear temperature rise through-the-thickness is considered, $p = 2$ leads to the highest values of critical buckling temperatures.

CONCLUSIONS

A thermal buckling analysis of functionally graded material (FGM) isotropic and sandwich plates was carried out by means of refined quasi-3D Equivalent Single Layer (ESL) and Zig-Zag (ZZ) plate theories developed within the framework of the Carrera Unified Formulation (CUF). Both the thermal stability differential equations with natural boundary conditions and the Hierarchical Trigonometric Ritz Formulation (HTRF) were derived by exploiting the use of the Principle of Virtual Displacements (PVD). Uniform, linear, non-linear temperature rises through-the-thickness direction were considered. The effects of significant parameters such as volume fraction index, length-to-thickness ratio, boundary conditions, aspect ratio, sandwich plate type and temperature distribution through-the-thickness direction on the critical temperatures were examined. From the analysis carried out, the following important conclusions can be drawn:

1. The developed advanced quasi-3D ESL and ZZ plate theories lead to more accurate results, in terms of critical temperature, when compared with CLPT, FSDT and HSDT.
2. For FGM isotropic and sandwich plates the critical temperatures decreased when increasing the thickness-to-length ratio (a/h).
3. For FGM sandwich plates the critical temperatures decreased when increasing the volume fraction index p if uniform or linear temperature rises through-the-thickness are taken into account, and increased when increasing the volume fraction index p if non-linear temperature rises through-the-thickness are accounted for.
4. The fully clamped boundary condition lead to higher critical temperatures than those obtained by using the simply supported one.
5. The critical temperature increased when increasing the temperature index χ.

6. From all of the considered non-linear temperature distributions through-the-thickness direction, the one obtained solving the one-dimensional Fourier heat conduction equation lead to the lowest critical buckling temperature.
7. From all of the considered FGM sandwich plate configurations, the 1-0-1 lead to the highest values of critical buckling temperatures.

REFERENCES

1. E. A. Thornton, Thermal Buckling of Plates and Shells, *ASME—Applied Mechanics Reviews*, vol. 46, no. 10, pp. 485–506, 1993.
2. T. R. Tauchert, Thermally Induced Flexure, Buckling, and Vibration of Plates, *ASME—Applied Mechanics Reviews*, vol. 44, no. 8, pp. 347–360, 1991.
3. C. C. Gray and C. Mei, Finite Element Analysis of Thermal Post-Buckling and Vibrations of Thermally Buckled Composite Plates, *AIAA Journal*, 1239-CP, vol. 4, pp. 2996–3007, 1991.
4. T. R. Tauchert, Thermal Buckling of Thick Antisymmetric Angle-Ply Laminates, *Journal of Thermal Stresses*, vol. 10, pp. 113–124, 1987.
5. I. H. Yang and J. A. Sheih, Generic Thermal Buckling of Initially Stressed Antisymmetric Cross-ply Thick Laminates, *International Journal of Solids and Structures*, vol. 24, pp. 1059–1070, 1988.
6. W. J. Chen, P. D. Lin, and L. W. Chen, Thermal Buckling Behavior of Thick Composite Laminated Plates under Nonuniform Temperature Distribution, *Computers & Structures*, vol. 41, pp. 637–645, 1991.
7. A. K. Noor and W. S. Jeanne, Predictor Corrector Procedures for Thermal Buckling Analysis of Multilayered Composite Plates, *Computers & Structures*, vol. 40, pp. 1071–1084, 1991.
8. M. R. Prabhu and R. C. Dhanaraj, Thermal Buckling of Laminated Composite Plates, *Computers & Structures*, vol. 53, no. 5, pp. 1193–1204, 1994.
9. A. K. Noor, J. M. Peters, and W. S. Burton, Three-Dimensional Solutions for Initially Stressed Structural Sandwiches, *ASCE Journal of Engineering Mechanics*, vol. 120, pp. 284–303, 1994.
10. A. K. Noor and W. S. Burton, Three-Dimensional Solutions for Thermal Buckling Multilayered Anisotropic Plates, *ASCE Journal of Engineering Mechanics*, vol. 118, pp. 638–701, 1992.
11. T. Kant and C. S. Babu, Refined High Order Finite Element Models for Thermal Buckling of Laminated Composite and Sandwich Plates, *Journal of Thermal Stresses*, vol. 23, pp. 111–130, 2000.
12. E. Carrera, Temperature Profile Influence on Layered Plates Response Considering Classical and Advanced Theories, *AIAA Journal*, vol. 40, no. 9, pp. 1885–1896, 2002.
13. E. Carrera, Transverse Normal Strain Effects on Thermal Stress Analysis of Homogeneous and Layered Plates, *AIAA Journal*, vol. 43, no. 10, pp. 2232–2242, 2005.
14. E. Carrera, An Assessment of Mixed and Classical Theories for the Thermal Stress Analysis of Orthotropic Multilayered Plates, *Journal of Thermal Stresses*, vol. 23, pp. 797–831, 2000.
15. E. Carrera and A. Ciuffreda, Closed-Form Solutions to Assess Multilayered-Plate Theories for Various Thermal Stress Problems, *Journal of Thermal Stresses*, vol. 27, pp. 1001–1031, 2004.
16. H. Matsunaga, Thermal Buckling of Angle-Ply Laminated Composite and Sandwich Plates According to High-Order Deformation Theory, *Composite Structures*, vol. 72, pp. 177–192, 2006.

17. A. K. Noor and W. S. Burton, Three-Dimensional Solutions for Thermal Buckling and Sensitivity Derivatives of Temperature-Sensitive Multilayered Angle-Ply Plates, *Journal of Applied Mechanics*, vol. 59, pp. 848–856, 1992.
18. S. Le-Chung, K. Shih-Yao, and C. Chen-Yuan, Thermal Buckling Behaviour of Laminated Composite Plates, *Composite Structures*, vol. 92, no. 2, pp. 508–514, 2010.
19. F. A. Fazzolari and E. Carrera, Advanced Variable Kinematics Ritz and Galerkin Formulations for Accurate Buckling and Vibration Analysis of Laminated Composite Plates, *Composite Structures*, vol. 94, no. 1, pp. 50–67, 2011.
20. F. A. Fazzolari and E. Carrera, Thermo-Mechanical Buckling Analysis of Anisotropic Multilayered Composite and Sandwich Plates by Using Refined Variable-Kinematics Theories, *Journal of Thermal Stresses*, vol. 36, no. 4, pp. 321–350, 2012.
21. A. M. Zenkour and M. Sobhy, Thermal Buckling of Various Types of FGM Sandwich Plates, *Composite Structures*, vol. 93, no. 1, pp. 93–112, 2010.
22. X. Zhao, Y. Y. Lee, and K. M. Liew, Mechanical and Thermal Buckling Analysis of Functionally Graded Plates, *Composite Structures*, vol. 90, no. 2, pp. 161–171, 2009.
23. W. Lanhe, Thermal Buckling of a Simply Supported Moderately Thick Rectangular FGM Plate, *Composite Structures*, vol. 64, no. 2, pp. 211–218, 2004.
24. H.-S. Shen, Thermal Post-Buckling Analysis of Imperfect Laminated Plates Using a Higher-Order Shear Deformation Theory, *International Journal of Non-Linear Mechanics*, vol. 32, no. 6, pp. 1035–1050, 1997.
25. B. Uymaz and M. Aydogdu, Three Dimensional Shear Buckling of FG Plates with Various Boundary Conditions, *Composite Structures*, vol. 96, no. 10, pp. 670–682, 2013.
26. P. Malekzadeh, Three-Dimensional Thermal Buckling Analysis of Functionally Graded Arbitrary Straight-Sided Quadrilateral Plates Using Differential Quadrature Method, *Composite Structures*, vol. 93, no. 4, pp. 1246–1254, 2011.
27. B. A. Samsam Shariat and M. R. Eslami, Buckling of Thick Functionally Graded Plates under Mechanical and Thermal Loads, *Composite Structures*, vol. 78, no. 3, pp. 433–439, 2007.
28. B. A. Samsam Shariat and M. R. Eslami, Thermal Buckling of Imperfect Functionally Graded Platess, *International Journal of Solids and Structures*, vol. 43, no. 14–15, pp. 4082–4096, 2006.
29. H. Matsunaga, Thermal Buckling of Functionally Graded Plates According to a 2D Higher-Order Deformation Theory, *Composite Structures*, vol. 90, no. 1, pp. 76–86, 2009.
30. F. A. Fazzolari, Fully Coupled Thermo-Mechanical Effect in Free Vibration Analysis of Anisotropic Multilayered Plates by Combining Hierarchical Plates Models and a Trigonometric Ritz Formulation, *Mechanics of Nano, Micro and Macro Composite Structures Politecnico di Torino Conference*, 18–20 June, 2012.
31. F. A. Fazzolari and E. Carrera, Accurate Free Vibration Analysis of Thermo-Mechanically Pre/Post-Buckled Anisotropic Multilayered Plates Based on a Refined Hierarchical Trigonometric Ritz Formulation, *Composite Structures*, vol. 95, pp. 381–402, 2013.
32. F. A. Fazzolari and E. Carrera, Coupled Thermoelastic Effect in Free Vibration Analysis of Anisotropic Multilayered Plates by Using an Advanced Variable-Kinematics Ritz Formulation, *European Journal of Mechanics Solid/A*, vol. 44, pp. 157–174, 2014.
33. F. A. Fazzolari and E. Carrera, Free Vibration Analysis of Sandwich Plates with Anisotropic Face Sheets in Thermal Environment by Using the Hierarchical Trigonometric Ritz Formulation, *Composites Part B: Engineering*, vol. 50, pp. 67–81, 2013.
34. F. A. Fazzolari and E. Carrera, Advances in the Ritz Formulation for Free Vibration Response of Doubly-Curved Anisotropic Laminated Composite Shallow and Deep Shells, *Composite Structures*, vol. 101, pp. 111–128, 2013.

35. A. E. H. Love, The Small Free Vibrations and Deformations of a Thin Elastic Shell, *Phil. Trans. Roy. Soc. (London), Ser. A*, vol. 179, pp. 491–549, 1888.
36. G. R. Kirchhoff, Über das Gleichgewicht und die Bewegung einer elastischen Sheibe. (About the equilibrium and motion of elastic bodies), *Journal für die Reine und Angewandte Mathematik*, vol. 40, pp. 51–88, 1850.
37. E. Reissner, The Effect of Transverse Shear Deformation on the Bending of Elastic Plates, *Journal of Applied Mechanics*, vol. 67, pp. A67–A77, 1945.
38. R. D. Mindlin, Influence of Rotary Inertia and Shear on Flexural Motions of Isotropic Elastic Plates, *Journal of Applied Mechanics*, vol. 18, no. 10, pp. 31–38, 1951.
39. E. Carrera and P. Nali, Multilayered Plate Elements for the Analysis of Multifield Problems, *Finite Elements in Analysis and Design*, vol. 46, pp. 732–742, 2010.
40. H. Murakami, Laminated Composite Plate Theory with Improved In-Plane Response, *Journal of Applied Mechanics*, vol. 53, pp. 601–666, 1986.
41. E. Carrera, Theories and Finite Elements for Multilayered Plates and Shells: A Unified Compact Formulation with Numerical Assessment and Benchmarking, *Archives of Computational Methods in Engineering*, vol. 10, no. 3, pp. 216–296, 2003.
42. W. Ritz, Über eine neue Methode zur Lösung gewisser Variationsprobleme der mathematischen Physik. (About a new method for the solution of certain variational problems of mathematical physics), *Journal für die Reine und Angewandte Mathematik*, vol. 135, pp. 1–61, 1909.
43. J. N. Reddy, *Energy Principles and Variational Methods in Applied Mechanics*, 2nd ed., John Wiley & Sons, Inc., Hoboken, New Jersey, 2002.
44. H. Nguyen-Xuan, Loc. V. Tran, T. Nguyen-Thoi, and H. C. Vu-Do, Analysis of Functionally Graded Plates Using an Edge-Based Smoothed Finite Element Method, *Composite Structures*, vol. 93, pp. 3019–3039, 2011.
45. R. Javaheri and M. R. Elsami, Thermal Buckling of Functionally Graded Plates Based on Higher Order Theory, *Journal of Thermal Stresses*, vol. 25, pp. 603–625, 2002.